Selective Electrocatalytic Reduction of 3-Nitrostyrene to 3-Vinylanaline over Pd- and Pt-based Nanoparticles

Chenxin Yang

Advisor: Sen Zhang

Committee Members: Ian Harrison, Charles Machan, Lin Pu

Abstract

Selective catalytic hydrogenation of organic molecules is one of the most critical processes in the fine chemical and pharmaceutical industries. Electrocatalytic hydrogenation (ECH) enables the controlled reduction of organic compounds under mild conditions with improved sustainability. This process requires high-performance electrocatalysts with satisfactory activity and selectivity. This study explores the use of Pd- and Pt-based alloy or intermetallic nanoparticles as electrocatalysts to enhance the selectivity and efficiency of 3-nitrostyrene (3-NS) conversion to 3-vinyl aniline (3-VA), a model reaction for the green chemical synthesis of functional aromatic amines.

A critical challenge of electrochemical 3-NS-to-3-VA conversion is the selectivity of the desired products. Our hypothesis is controlling electrochemical reaction conditions (pH and potentials) and catalyst binding energies with reactants and intermediates could lead to improved selectivity. In our study, the electrocatalytic performances of commercial Pd and Pt catalysts were first evaluated using different pH conditions and reduction potentials, and we found that the neutral condition could achieve a higher selectivity at the same potential comparing to acidic or alkaline conditions. Furthermore, to enhance the selectivity to 3-VA rather than other deeply reduced products (3-ethylaniline (3-EA) and 1-ethyl-3-nitrobenzene (3-EN)),

nanoparticles including CuPd, CoPt, Co_2P and Co_2P/Pt were studied, demonstrating the potential of alloying and heterostructure effects in weakening the adsorption energy of reaction intermediates and minimizing the formation of deeply reduced products. These catalysts enhanced selectivity for 3-VA, achieving over 80% at -0.45 V (vs. RHE), which were significantly better than monometallic and commercial Pt and Pd catalysts (< 40%).

The future work will focus on further improvement of catalytic activity, selectivity and detailed characterization, like *in situ* analysis, to understand structural and compositional changes of the catalysts during the reaction. Computational work (e.g., DFT) will also be pursued to understand how the catalysts' atomic structures influence the reaction pathways and performances. The efficacy of this technology for other functional amine production will also be investigated. These insights will aid in designing more efficient and selective electrocatalysts for the industrial production of functionalized aromatic amines.

Acknowledgements

I would like to express my deepest gratitude to my advisor, Prof. Sen Zhang. Although I did not pass the candidacy, he showed great patience and trust in my ability. For improving my basic knowledge, he helped me in suggesting textbook, offering lunch meeting as an opportunity to learn electrochemistry, etc. I am thankful for the chance to participate in a training session in membrane electrode assembly in North Carolina, which have significantly enhanced my research skills. I hope to continue making progress under Prof. Zhang's mentorship in the future.

Gratitude is also extended to Prof. Pu for his guidance in organic chemistry during our biweekly group meetings. His insights and suggestions have greatly enriched my understanding of the subject. Heartfelt thanks go to Yichen Li for her assistance with NMR data analysis, which was crucial for the accurate interpretation of my experimental results. I am also deeply grateful for my committee members, Prof. Ian Harrison, Prof. Charles Machan for their willingness to participate in my M.S. thesis defense and for providing help throughout.

I also extend my thanks to Daniel Musikanth, Dr. Xiangru Wei, and Liyue Zhang for their invaluable help in catalyst synthesis, providing me with the necessary materials and expertise to advance my research. I would like to thank Dr. Yizhen Chen for his strong support in both work and experiments. His willingness to

patiently answer all my questions has been immensely helpful. I would like to thank Dr. Weijie Zhang for his help in understanding the advancements in thermal catalysis for the reduction of 3-NS, which provided broader and deeper insights into my own work.

Furthermore, I want to extend my gratitude to Dr. Earl Ashcraft. He helped me a lot in dealing problems from high performance liquid chromatography (HPLC) and, most importantly, was willing to lend me the column during these months.

Lastly, I am deeply grateful to my parents for their unwavering support and understanding throughout these past six months. Their encouragement has been a constant source of strength and motivation, helping me move forward without giving up.

Table of Contents

Chapter 1

Overview of Selective Reduction for Functionalized Aromatic Amines

1.1 Background and motivation

Functional aromatic amines and their derivatives are important and valuable industrial raw materials and chemical intermediates, for example, for the synthesis of medicines like Tylenol, dyes used in jeans production, etc[1-4](see **Table 1.1** for more examples). In 1826, German chemist Otto Unverdorben first obtained aniline from the herb indigo by dry distillation separation technology. After 15 years, Russian chemist Nikolay N. Zinin first obtained aniline by nitrobenzene reduction. Since then, researchers have continuously worked to design various catalytic systems that are efficient and highly selective for nitroaromatics conversion[5-7]. However, in industrial production, stoichiometric reducing agents like iron in acidic media or tin chloride are still commonly used to hydrogenate nitroaromatic through non-catalytic direct redox processes. These methods not only have low selectivity but also generate significant amounts of environmentally harmful metal waste.[5, 7]

Table 1.1 Application of aromatic amines

Name	Chemical formula	Structural formula	Application
o-Toluidine	C_7H_9N	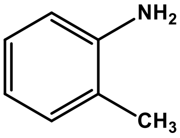	Dyes, pesticides, pharmaceuticals

o-Chloroaniline	C_6H_6ClN	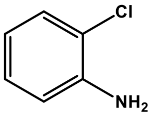	Synthetic resin intermediates
Diphenylamine	$C_{12}H_{11}N$	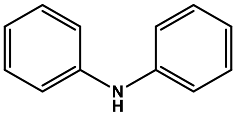	Antioxidants, rubber antioxidants
p-Aminophenol	C_6H_7NO	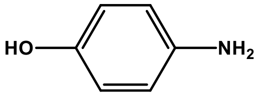	Dye intermediates
1-Hydroxy-4-chloroaniline	C_6H_6ClNO	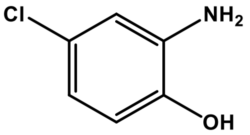	Pharmaceutical intermediates

Scientists have focused on the selective reduction of nitroaromatic via thermal catalysis[8, 9]. These reactions typically occur under high temperature and pressure, using hydrogen gas as the hydrogen source. While thermal catalysis can achieve high selectivity, major drawbacks like the stringent experimental conditions, high catalyst costs, and safety concerns still exist. Additionally, using hydrogen source from methane steam reforming poses environmental pollution issues, which do not satisfy the green chemistry requirements.

To address these issues, we have turned to electrocatalytic hydrogenation for the reduction of nitro groups. This method operates under mild conditions, using sustainable electricity as the driving energy and water as the hydrogen source. This approach ensures a more environmentally friendly and efficient reduction process.

Pt group metals are common choices of heterogeneous catalysts for reduction reaction. However, nitroaromatic compounds often contain other reducible groups such as C=C, C=O, C≡C, and C≡N. Traditional platinum group metal catalysts tend to reduce these unsaturated groups along with the nitro group. Therefore, the rational design of catalysts that can precisely control the hydrogenation of nitro groups remains a significant challenge.

From the study of thermocatalysts design for 3-NS-to-3-VA reaction, one effective strategy is to introduce fewer active components into platinum group metals. For example, catalysts like $Pd_{13}Pb_9$, PtZn, and PtSn not only exhibit high activity in the selective hydrogenation of nitrobenzene but also demonstrate high chemoselectivity for aminostyrene[10]. Through precise design, platinum group metal atoms can be isolated on the surface of less active metals. This unique alloying pattern significantly alters the electronic structure of the isolated metal atoms, resulting in notable improvements in activity, selectivity, and stability compared to traditional metal catalysts[11]. We hypothesize the strategy may also by applicable in designing electrocatalysts. Considering Pt groups metals normally has great performance in HER, alloying may also inhibit it and improve the faradaic efficiency 3-NS-to-3VA reaction accordingly. However, there is still limited research on designing electrocatalysts for selective ECH of 3-NS by using analogous strategy in catalysts design in other reduction methods. Therefore, by reviewing the design strategy of 3-

NS-to-3-VA catalysts from other reduction methods, it is significantly helpful for us to preliminarily screen out electrocatalysts that can effectively improve the selectivity in this reaction.

1.2 Nitroaromatic reduction method

Several methods have been developed to facilitate nitroaromatic reduction conversion, each with unique mechanisms, advantages, and limitations. This section will provide an overview of these methods, focusing on their principles and applications.

1.2.1 Direct redox method

The direct redox method for nitroaromatic reduction involves using stoichiometric reducing agents like iron in acidic media or tin chloride. For example, the Bechamp reduction process uses iron and hydrochloric acid to produce aniline from nitrobenzene but has a selectivity lower than 50%, generating significant iron oxide waste. In 2020, the global production of aniline was approximately 6 million tons, with a substantial portion derived from such inefficient methods. Despite being cost-effective, these processes are environmentally detrimental, prompting the need for greener alternatives in industrial applications.

1.2.2 Thermal catalytic reduction method

Thermal catalytic reduction is the method of reducing nitroaromatics to their corresponding aromatic amines through the combined action of a catalyst and a hydrogen source (**Figure 1.1**). Commonly used catalysts include noble metals (such as Au, Ag, Pt, and Pd *et al* [12-15]). There are many types of hydrogen sources, including gaseous sources like hydrogen (H_2)[16-18] and syngas (CO/H_2O) [19], liquid hydrogen sources like hydrazine hydrate ($N_2H_4.H_2O$) [20-22], formic acid (HCOOH) [23-26], alcohol [27, 28], etc.

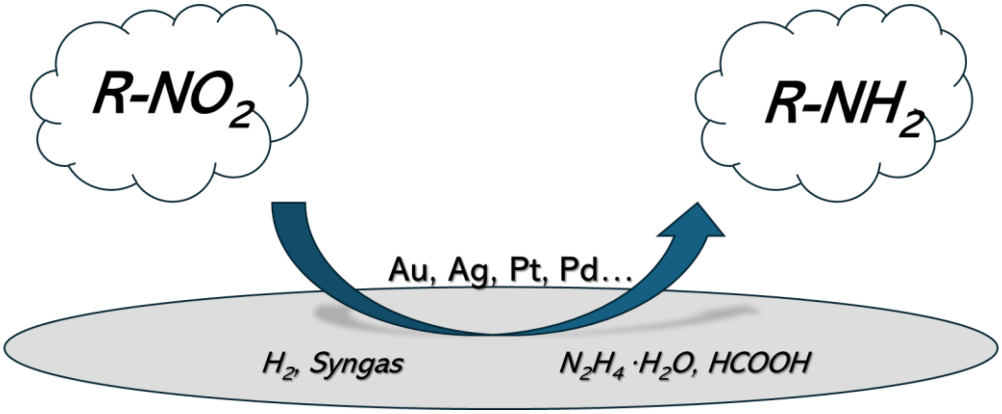

Figure 1.1 The scheme of nitroaromatic hydrogenation over catalysts with different hydrogen sources.

1.2.2.1 gaseous *hydrogen source (H_2 and syngas)*

Hydrogen (H_2) and syngas are widely used as a hydrogen source in the industry production[29]. People commonly employ metals or their oxides as catalysts. The typical hydrogenation condition is under high pressure and temperature. Due to the safety concern, high gas pressure presents an obstacle to the further development in aromatic nitrate thermal reduction. Therefore, it is highly focused on finding efficient and mild catalytic systems for the hydrogenation of nitroaromatics. With the advancement in this field, catalytic systems have recently been developed that enable the hydrogenation of nitroaromatics at low pressure and low temperature, as shown in **Figure 1.2**. Ma *et al*. investigated the electrocatalytic hydrogenation of nitroaromatics using platinum single atoms on CeO_2, modified with phosphorus to enhance hydrogenation activity. The reaction condition is set in 1 bar and temperature is around 50℃. They found that this modification improved the catalyst's selectivity (over 80%) for hydrogenating nitro groups over other functional groups, such as $C=C$, $C=O$, and $C\equiv C$. Nonetheless, the use of flammable and explosive gas still carries certain risks, especially under heating and pressurization. Consequently, it is particularly important to develop highly efficient catalysts which are capable of selectively catalyzing nitroaromatics under mild conditions.

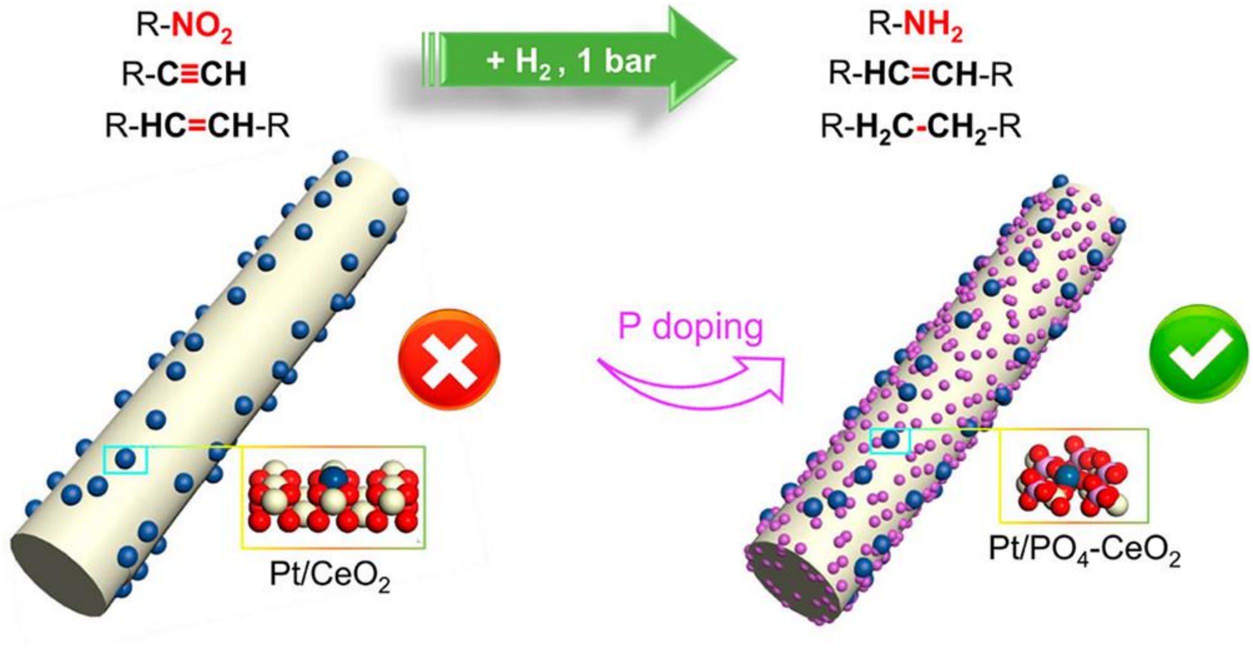

Figure 1.2. By tailoring the local coordination environment of Pt single atoms on phosphorus-doped CeO_2 enhances catalytic activity up to tenfold under hydrogen as hydrogen source condition[30].

1.2.2.2 Liquid hydrogen sources (Hydrazine hydrate, HCOOH, etc)

Hydrazine hydrate, as a stable hydrogen donor and relatively inexpensive reagent, offers advantages such as mild reaction conditions, high conversion rates. Researchers are committed to enhancing the reaction efficiency and selectivity of hydrazine hydrate in reducing nitro compounds. Though many noble metals (such as Pt, Au, Pd/C) exhibit excellent catalytic performance for this reaction, the cost of these catalysts limits their industrial application. Consequently, researchers have focused on developing low-cost transition metal catalysts to replace noble metals in the hydrogenation of nitroaromatics using hydrazine hydrate, as shown in **Figure**

1.3. The research groups led by Hailong Jiang[31] and Zhengping Dong[32] have successfully synthesized γ-Fe_2O_3 nanoparticles encapsulated in porous carbon via a metal-organic framework-templated pyrolysis. This catalyst demonstrated excellent chemoselectivity and efficiency for the hydrogenation of nitro compounds under ambient pressure. The catalyst achieved selectivity over 99% for the hydrogenation of nitrobenzene to aniline at 85℃. However, the use of organic solvents may bring recycle problem and excessively high reaction temperatures still limits the widespread application of hydrazine hydrate technology[31-33].

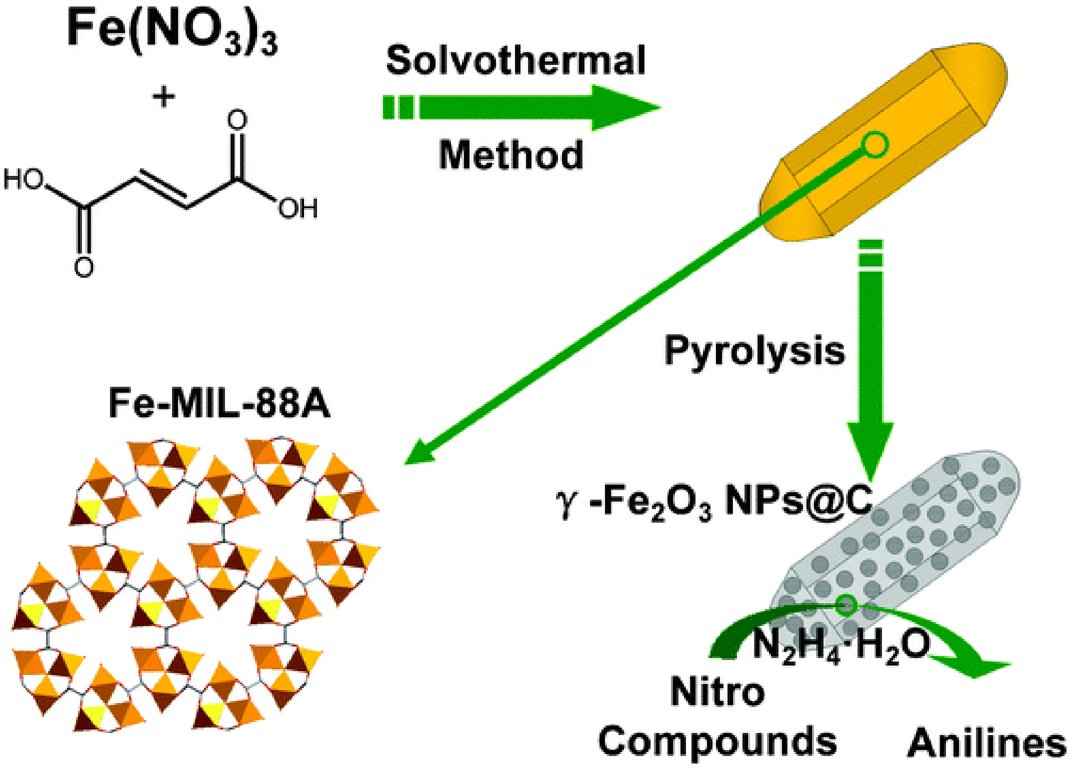

Figure 1.3 γ-Fe_2O_3 nanoparticles in porous carbon, fabricated via MOF-templated pyrolysis, exhibit excellent catalytic activity and chemoselectivity for nitro compound hydrogenation with hydrazine hydrate as hydrogen source[31]

1.2.3 Photo catalytic reduction

Photocatalytic reduction utilizes the power of photogenerated electrons from electron-hole pairs in semiconductors under light excitation, converting light into chemical energy for organic synthesis and reduction[34]. This green method includes innovations like the Au-Cu@ZrO_2 and Pd-Au nanorod photocatalysts for effective hydrogenation of nitroaromatics under visible light[35, 36]. However, the technique often requires organic solvents to enhance substrate diffusion due to the poor water solubility of many nitroaromatics, which poses environmental challenges[36, 37]. Additionally, the process frequently involves sacrificial agents to overcome the rapid recombination of photogenerated charges, which can limit efficiency.

1.2.4 Electrocatalytic reduction

In recent years, the electrochemical reduction of nitroaromatics has garnered significant attention from researchers. This method mainly uses protons from water, offering advantages such as controllable reducing potentials and improved environmental sustainability in the synthesis of aromatic amines[38, 39]. The reaction is typically conducted in a three-electrode, two-compartment cell. In this setup, the cathodic reaction reduces nitroaromatics to aniline, while the anodic reaction involves water oxidation. The protons generated from water oxidation ($2H_2O \rightarrow 4H^+ + O_2$) combine with electrons to drive the hydrogenation process. This typically occurs within the potential range of hydrogen evolution from water splitting (0 V vs. RHE), making the reduction of nitroaromatics and water competitive reactions (HER). Key parameters in the electrocatalytic hydrogenation of nitroaromatics include applied potential, current density, faradaic efficiency, product selectivity, and catalyst stability, as in other electrocatalytic processes[38].

Currently, research on the electrocatalytic reduction of nitroaromatics is still in its early stages. **Table 1.2** lists catalysts used in recent years for the ECH of nitroaromatics, along with their performance. We found that most of these studies focus on the ECH of nitrophenol or nitrobenzene, which do not involve another reducible functional group (e.g. C=C, C=O, C≡C). Notably, only Zhang *et al.* in 2023 successfully achieved the selective reduction of 4-nitrostyrene to 4-vinyl aniline by using Pd-Mo metallene at -0.25 V vs. RHE, with over 90% selectivity for the nitro group reduction to an amino group. However, their work did not sufficiently expand to different substrates such as those reducible functional groups at ortho- or meta- positions.

Table 1.2 Performance summary of various recently developed catalysts for the ECH of nitroaromatic.

Electrocatalyst	**E (V vs RHE)**	**Reactions**	**Selectivity (%)**
Au micropillars	-0.072	PNP → PAP	100[40]
Cu_xPt_y/C	-0.3	NB → AB	99[41]
Pd-Mo	-0.25	4-NS → 4-VA	90[42]
Ru-PA/NF	-1.6	PNP → PAP	99[43]
CoPt nanowires	-0.15	PNP → PAP	medium[44]

CFC: carbon felt cloth; PNP: *p*-nitrophenol; PAP: *p*-aminophenol; NB: nitrobenzene; AB: aminobenzene; 4-NS:4-nitrostyrene; 4-VA:4-vinyl aniline.

1.3 Catalysts for hydrogenation of nitroaromatics

As we mentioned in 1.1, by using analogous strategy in catalysts design in other reduction methods will contribute to the electrocatalyst structure design for selective ECH of 3-NS. The catalysts investigated for selective catalytic hydrogenation of nitroaromatics using H_2 include metals and metal oxides. In the following sections, we will review these catalysts, emphasizing how to optimize their structure and composition to achieve high activity and selectivity.,

1.3.1 Metal

Metals such as Pt, Pd, Ru, Ni, and Co exhibit high activity for nitroaromatic hydrogenation reactions. However, they often cannot differentiate between nitro groups and other competing functional groups like alkenes. Various strategies have been explored to enhance selectivity, including size effects, alloying effects, strain effects, and interfacial adsorbate-metal interactions, etc.

1.3.1.1 Size effect

Different metal coordination sites (terrace, edge, kink, or corner)[45] on metal nanoparticles show varied abilities for H_2 dissociation due to their distinct surface structures and electronic properties, resulting in different hydrogenation activities[46]. The distribution of these sites typically depends on the nanoparticle size, with smaller nanoparticles enhancing selectivity by favoring nitro group adsorption over other functional groups.

Duan *et al* studied Pd catalysts of different sizes were supported on carbon nanotubes (CNT) to explore the structure sensitivity in the hydrogenation of 2,6-diamino-3,5-dinitropyridine (DADNP)[47]. Kinetic tests revealed that the apparent activation energies for DADNP conversion were not sensitive to Pd catalyst sizes of 2.6 nm or larger, suggesting that a single type of active site drives the hydrogenation process. Model calculations and multi-facet kinetic analysis, based on the identified shape of Pd nanoparticles (**Figure 1.4(a)**), indicated that the normalized turnover frequencies (TOFs) for DADNP were independent of Pd particle size when based on the number of (111) sites, identifying Pd (111) as the dominant active site for DADNP conversion (**Figure 1.4(b)**). For Pd catalysts smaller than 2.6 nm, both kinetic analyses and X-ray photoelectron spectroscopy measurements suggested that catalytic performance was influenced primarily by electronic properties. Understanding these size effects, particularly the structure sensitivity, is crucial for designing high-performance catalysts.

It's important to note that size effects are not only linked to the catalytic performance influenced by the size of active metal particles but also involve both electronic and geometric contributions. Specifically, reducing the size of active metal nanoparticles can alter the electronic properties of active sites, thereby modifying the adsorption and activation of reactants and potentially changing the reaction pathway from producing the target product to forming side products. Conversely, increasing the size of metal nanoparticles can reduce the number of low-coordination surface sites and increase high-coordination sites, which can change the adsorption configuration of reactants and shift the reaction pathways accordingly.

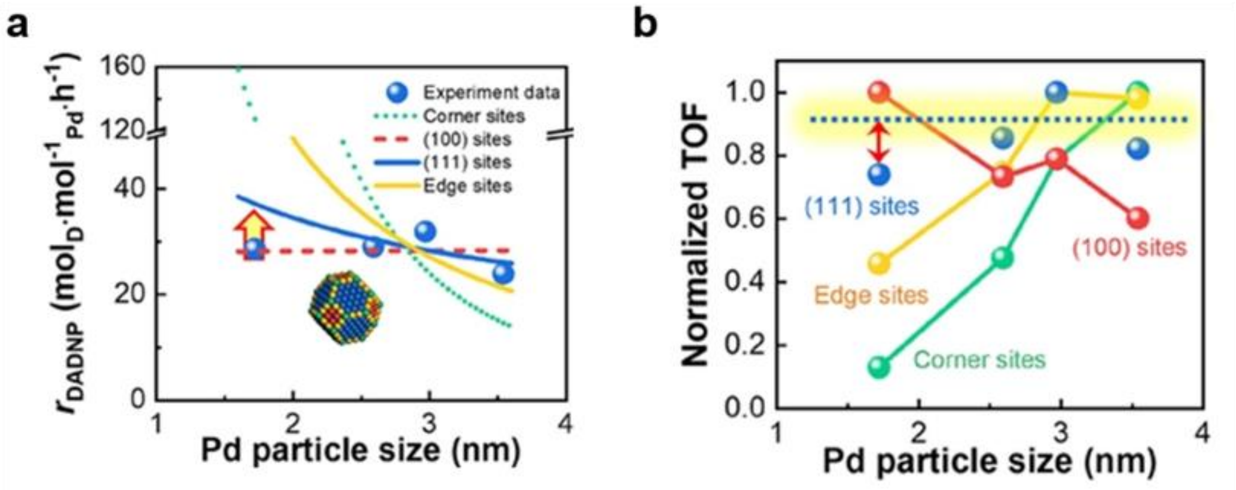

Figure 1.4 (a) Comparison of the experimental and calculated reaction rate by the fitted r_{corner}, r_{edge}, $r_{(100)}$, and $r_{(111)}$ plots of normalized TOFs for DADNP conversion as function of Pd size. **(b)** Plots of normalized TOFs for DADNP conversion as function of Pd size[47].

1.3.1.2 Alloy and strain effect

Gold (Au) exhibits high selectivity for the hydrogenation of nitroaromatics, but its activity is limited by the kinetics of H_2 dissociation. In contrast, other metals like Pt and Pd can easily dissociate H_2[48]. Therefore, bimetallic catalysts such as Pt-Au and Pd-Au supported on TiO_2 have been explored to enhance the selective hydrogenation of nitroaromatics[49]. The formation of alloys can cause compression or expansion of surface atoms, altering lattice strain and thus affecting catalytic activity[50, 51].

Recent studies show that adjusting the lattice strain of metal catalysts can influence their catalytic properties by changing their electronic structure, which affects the adsorption of reactants and the activation energy of transition states[52, 53]. For instance, Li *et al*. reported the use of dumbbell-shaped Co-Ru nanostructures for the selective hydrogenation of 4-nitrostyrene[54]. This structure comprises Co nanorods with Ru nanoplate ends, where the Ru lattice is compressed due to the central Co connection. As a result, $Co_{0.46}$-$Ru_{0.54}$ nanoparticles produced significant amounts of 4-nitroethylbenzene and 4-aminostyrene, while $Co_{0.12}$-$Ru_{0.88}$ and $Co_{0.38}$-$Ru_{0.62}$ showed lower selectivity for 4-nitroethylbenzene. Remarkably, $Co_{0.23}$-$Ru_{0.77}$ exhibited no 4-nitroethylbenzene, indicating specific hydrogenation selectivity for the NO_2 group. Interestingly, the selectivity for 4-aminostyrene correlated with the compressive lattice strain of Ru in a volcano-shaped relationship. Pure Ru's selectivity was 66%, which increased to 99% when the Ru lattice was compressed by 3% (from 2.14 to 2.08 Å). Further compression led to decreased selectivity. DFT calculations indicated that the optimal transverse compressive strain (3%) favored the hydrogenation of the NO_2 group while hindering the hydrogenation of the C=C group.

1.3.1.3 Interfacial adsorbate-metal interaction

Recent suggestions have focused on using organic/inorganic adsorbates to modify the electronic properties of active metals[54]. For instance, Zheng *et al.* synthesized ethylenediamine (EDA) coated ultrathin Pt nanowires (EDA-Pt NWs) and demonstrated that organic adsorbates on the metal surface can induce significant interfacial electronic effects, influencing catalytic selectivity[45]. This catalyst exhibited unexpectedly high selectivity for the production of phenylhydroxylamine, a thermodynamically unfavorable but industrially important chemical. At full conversion of nitrobenzene, the selectivity reached nearly 100% within 50 minutes and remained high even when the reaction time was extended to 2 hours. In contrast, unmodified Pt could not achieve such high selectivity. DFT calculations indicated that the electron-donating nature of EDA renders Pt highly electron-rich, which favors the adsorption of electron-deficient reactants like phenylhydroxylamine and prevents its complete hydrogenation to aniline. This showcases how tuning the electronic environment of catalysts through surface modifications can significantly en

1.3.2 Metal oxide

Metal oxides are often used as supports to anchor active metal sites, controlling the overall hydrogenation performance, including selectivity and reaction rate[55]. For example, the hydrogenation of nitrobenzene on Au/TiO_2 follows a direct pathway, while on Au/CeO_2 it proceeds via a condensation pathway[56]. The condensation route requires a high concentration of nitrosobenzene. In the case of Au/TiO_2, nitrosobenzene rapidly converts to phenylhydroxylamine, which accumulates on the surface before being converted to aniline, preventing the formation of azoxybenzene. Conversely, Au/CeO_2 shows a much slower hydrogenation rate, leading to the accumulation of nitrosobenzene and the formation of condensation intermediates. All these catalysts require active metal phases, such as Au and Au-Pt alloys, to facilitate H_2 dissociation.

Recently, certain oxygen-deficient and nitrogen-doped metal oxides have been reported to exhibit the ability to dissociate H_2, expanding the potential for designing selective hydrogenation catalysts. For instance, these modified metal oxides can provide unique electronic environments that enhance the performance of supported metal nanoparticles, improving both selectivity and activity in hydrogenation reactions[57].

1.4 Overview of reaction mechanisms for aromatic amines hydrogenation

1.4.1 Thermal catalytic reaction mechanism

100 years ago, Haber and others proposed a direct deoxygenation mechanism for nitrobenzene, namely PhNO2 → PhNO* → PhNHOH* → $PhNH_2$ (**Figure 1.5(a)**)[58]. They hypothesized that these species could reach equilibrium in water and undergo reversible adsorption on the surface of solid catalysts. The diagram below describes the reaction mechanism in catalytic hydrogenation reactions (**Figure 1.5**). According to Raman spectroscopy and infrared spectroscopy analysis, only nitroaromatics,

nitroso compounds, hydroxylamine, and aniline products can be detected in aqueous solutions[59]. The concentration of nitroso intermediates is very low, and the concentration of hydroxylamine is influenced by the substrate structure, reaction temperature, hydrogen pressure, agents, oxidizers, and pH value. The reaction shows that nitro groups can be rapidly reduced to nitroso intermediates and strongly adsorbed onto the metal surface, subsequently being rapidly hydrogenated to hydroxylamine, while the hydrogenation of hydroxylamine to aniline is the rate-determining step of the reaction.

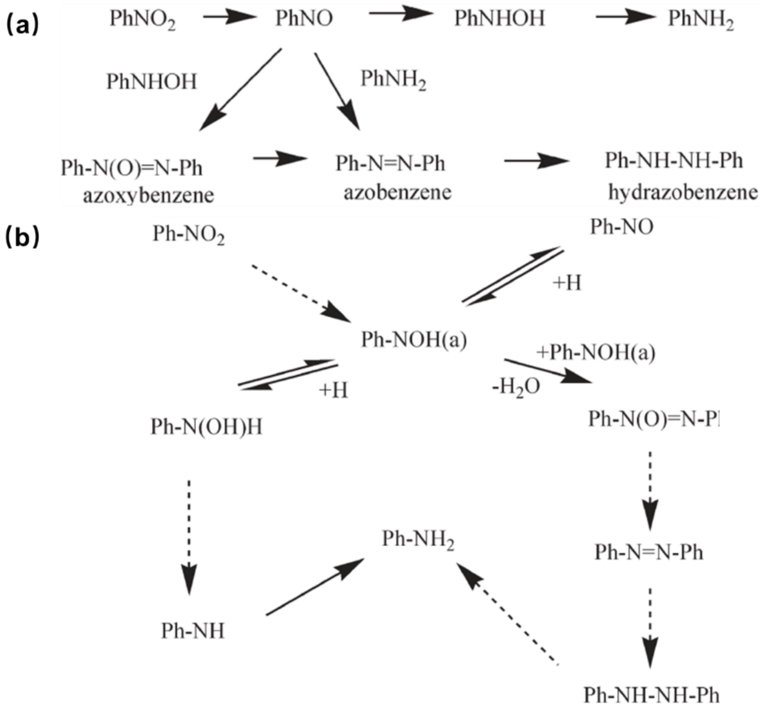

Figure 1.5 (a) Haber nitrobenzene hydrogenation mechanism; **(b)** Jackson nitrobenzene hydrogenation mechanism.

Contrary to the mechanisms mentioned above, Jackson *et al.* found that when nitrosobenzene is used as the starting substrate, there is a noticeable change in the reaction curve, indicating that the nitroso group is not a necessary intermediate in the reaction, and a direct pathway from nitro to hydroxylamine might exist (**Figure 1.5(b)**)[60, 61]. They believe that during the gasification process of nitrobenzene, Ph-N(OH) is a common intermediate (**Figure 1.5(b)**), where Ph-N(OH) combines with hydrogen atoms adsorbed on the catalyst surface to form Ph-NH and ultimately Ph-NH_2, and two molecules of Ph-N(OH) dehydrate to form oxyazobenzene. However, it does not explain how to add four atoms to the nitro group and lose one molecule of water in a single-step reaction. In 2014, Biswarup Pathak[62] *et al.* were the first to study both reaction mechanisms on the surface of a Ni catalyst (**Figure 1.6**), showing that surface Ph-NO is more inclined to convert to Ph-NHOH via a Ph-NOH intermediate rather than through a Ph-NHO intermediate. Elementary reaction barrier data shows that the conversion of nitrobenzene to aniline can follow either a direct or an indirect reaction pathway. However, the reaction tends to favor the direct pathway because this pathway involves spontaneous elementary reactions and has a lower thermodynamic barrier.

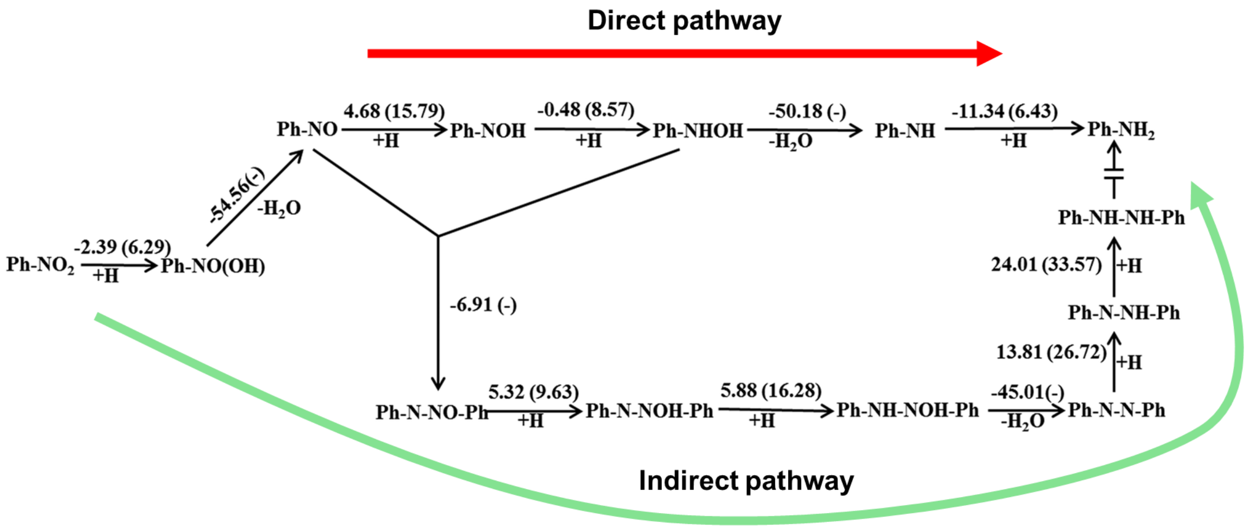

Figure 1.6 The direct and indirect pathways of nitrobenzene reduction reaction with calculated spin polarized and dispersion corrected reaction energies and activation barriers (values in parentheses) for the elementary steps.[62].

1.4.2 Electro catalytic reaction mechanism

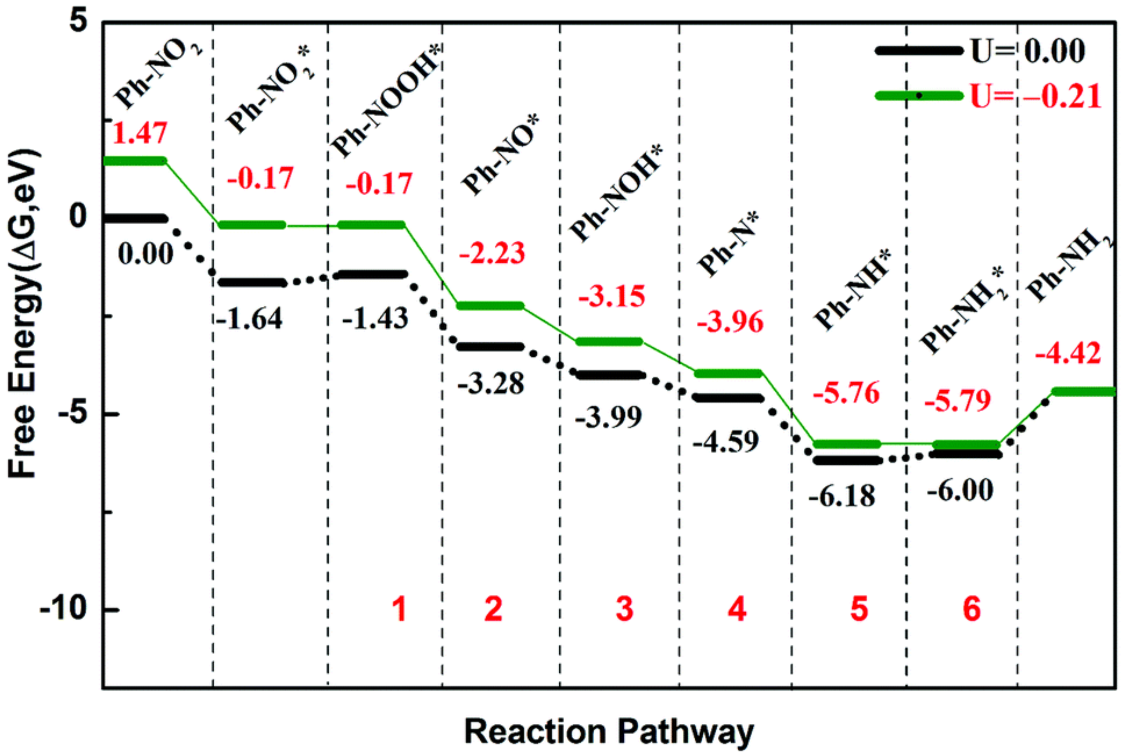

Figure 1.7 The computed Gibbs free energy diagrams for nitrobenzene reduction to aniline on the PtN_3/G surface at zero and applied potentials[63].

In 2020, Zhao and others studied the electrocatalytic hydrogenation reaction process of nitrobenzene on nitrogen-doped graphene containing different transition metal atoms (TMN/GTM = Ni, Cu, Pd, Pt). The study showed that after the adsorption of nitrobenzene, the reaction follows an indirect hydrogen-assisted reaction pathway, because the energy barrier for the first step of direct hydrogenation to form the Ph-NOOH* intermediate is lower than the barrier for direct deoxygenation to form Ph-NO* (**Figure 1.7**)[63]. However, this work did not explore in depth the effects of applied potential and solution pH on product selectivity. Zhang *et al.* thoroughly investigated how reaction conditions such as applied potential and solution pH affect product selectivity in the CuPt alloy catalyst system. In their work, it was proposed that after nitrobenzene molecules are adsorbed onto the catalyst surface, the first step is more likely to follow a direct deoxygenation pathway to form Ph-NO*, and Ph-NO* continues to deoxygenate to form the Ph-N* reaction intermediate, naming this pathway as the direct deoxygenation and then hydrogenation reaction pathway (SDR).

1.5 Reference

1. Lan, X.; Ali, B.; Wang, Y.; Wang, T., Hollow and Yolk–Shell Co-N-C@SiO2 Nanoreactors: Controllable Synthesis with High Selectivity and Activity for Nitroarene Hydrogenation. *ACS Applied Materials & Interfaces* **2020,** *12* (3), 3624-3630.

2. Goswami, A.; Kadam, R. G.; Tuček, J.; Sofer, Z.; Bouša, D.; Varma, R. S.; Gawande, M. B.; Zbořil, R., Fe (0)-embedded thermally reduced graphene oxide as efficient nanocatalyst for reduction of nitro compounds to amines. *Chemical Engineering Journal* **2020,** *382*, 122469.

3. Wang, H.; Li, X.; Cui, Z.; Yang, L.; Sun, S., Tobacco stem-derived N-enriched active carbon: efficient metal free catalyst for reduction of nitroarene. *Reaction Kinetics, Mechanisms and Catalysis* **2020,** *130*, 331-346.

4. Kumar, A.; Paul, B.; Boukherroub, R.; Jain, S. L., Highly efficient conversion of the nitroarenes to amines at the interface of a ternary hybrid containing silver nanoparticles doped reduced graphene oxide/graphitic carbon nitride under visible light. *Journal of hazardous materials* **2020,** *387*, 121700.

5. Sun, S.; Du, M.; Zhao, R.; Jv, X.; Hu, P.; Zhang, Q.; Wang, B., Zn (0)-Catalysed mild and selective hydrogenation of nitroarenes. *Green Chemistry* **2020,** *22* (14), 4640-4644.

6. Sahoo, L.; Mondal, S.; Nayana, C.; Gautam, U. K., Facile d-band tailoring in Sub-10 nm Pd cubes by in-situ grafting on nitrogen-doped graphene for highly efficient organic transformations. *Journal of Colloid and Interface Science* **2021,** *590*, 175-185.

7. Yoo, B.-W.; Kim, D.-I.; Kim, H.-M.; Kang, S.-H., Efficient and Selective Reduction of Aromatic Nitro Compounds to Aromatic Amines by NbCl 5/Indium System. *Bulletin of the Korean Chemical Society* **2012,** *33* (9), 2851-2852.

8. Göksu, H.; Zengin, N.; Burhan, H.; Cellat, K.; Şen, F., A novel hydrogenation of nitroarene compounds with multi wall carbon nanotube supported palladium/copper nanoparticles (PdCu@ MWCNT NPs) in aqueous medium. *Scientific reports* **2020,** *10* (1), 8043.

9. Liu, L.; Corma, A., Metal catalysts for heterogeneous catalysis: from single atoms to nanoclusters and nanoparticles. *Chemical reviews* **2018,** *118* (10), 4981-5079.

10. Feng, H.; Liu, W.; Wang, L.; Xu, E.; Pang, D.; Ren, Z.; Wang, S.; Zhao, S.; Deng, Y.; Liu, T.; Yang, Y.; Zhang, X.; Li, F.; Wei, M., Rational Design and Precise Synthesis of Single-Atom Alloy Catalysts for the Selective Hydrogenation of Nitroarenes. *Advanced Science* **2024,** *11* (23), 2304908.

11. Dai, Y.; Li, C.; Shen, Y.; Zhu, S.; Hvid, M. S.; Wu, L.-C.; Skibsted, J.; Li, Y.; Niemantsverdriet, J. H.; Besenbacher, F., Efficient solar-driven hydrogen transfer by bismuth-based photocatalyst with engineered basic sites. *Journal of the American Chemical Society* **2018,** *140* (48), 16711-16719.

12. Monti, G. A.; Correa, N. M.; Falcone, R. D.; Silbestri, G. F.; Moyano, F., Water-soluble gold nanoparticles: recyclable catalysts for the reduction of aromatic nitro compounds in water. *RSC advances* **2020,** *10* (26), 15065-15071.

13. Varshney, S.; Bar-Ziv, R.; Zidki, T., On the remarkable performance of silver-based alloy nanoparticles in 4-nitrophenol catalytic reduction. *ChemCatChem* **2020,** *12* (18), 4680-4688.

14. Van Thuan, D.; Khoa, N. T.; Kim, S.-W.; Chung, J. S.; Hur, S. H.; Kim, E. J.; Hahn, S. H.; Wang, M., Photo-enhanced selective reduction of nitroarenes over Pt/ZnO catalyst. *Catalysis Letters* **2017,** *147*, 2440-2447.

15. Kiani, Z.; Zhiani, R.; Khosroyar, S.; Motavalizadehkakhky, A.; Hosseiny, M., UiO-66/btb/Pd as a stable catalyst reduction of 4-nitrophenol into 4-aminophenol. *Inorganic Chemistry Communications* **2021,** *124*, 108382.

16. She, W.; Qi, T.; Cui, M.; Yan, P.; Ng, S. W.; Li, W.; Li, G., High catalytic performance of a CeO2-supported Ni catalyst for hydrogenation of nitroarenes, fabricated via coordination-assisted strategy. *ACS applied materials & interfaces* **2018,** *10* (17), 14698-14707.

17. Liu, L.; Concepción, P.; Corma, A., Modulating the catalytic behavior of non-noble metal nanoparticles by inter-particle interaction for chemoselective hydrogenation of nitroarenes into corresponding azoxy or azo compounds. *Journal of Catalysis* **2019,** *369*, 312-323.

18. Aygün, M.; Chamberlain, T. W.; Gimenez-Lopez, M. d. C.; Khlobystov, A. N., Magnetically recyclable catalytic carbon nanoreactors. *Advanced Functional Materials* **2018,** *28* (34), 1802869.

19. Zhou, P.; Yu, C.; Jiang, L.; Lv, K.; Zhang, Z., One-pot reductive amination of carbonyl compounds with nitro compounds with CO/H2O as the hydrogen donor over non-noble cobalt catalyst. *Journal of catalysis* **2017,** *352*, 264-273.

20. Liao, C.; Liu, B.; Chi, Q.; Zhang, Z., Nitrogen-doped carbon materials for the metal-free reduction of nitro compounds. *ACS applied materials & interfaces* **2018,** *10* (51), 44421-44429.

21. Huang, H.; Tan, M.; Wang, X.; Zhang, M.; Guo, S.; Zou, X.; Lu, X., Synthesis of mesoporous γ-alumina-supported Co-based catalysts and their catalytic performance for chemoselective reduction of nitroarenes. *ACS applied materials & interfaces* **2018,** *10* (6), 5413-5428.

22. Wei, Q.; Qin, F.; Ma, Q.; Shen, W., Coal tar-and residual oil-derived porous carbon as metal-free catalyst for nitroarene reduction to aminoarene. *Carbon* **2019,** *141*, 542-552.

23. Shalom, M.; Molinari, V.; Esposito, D.; Clavel, G.; Ressnig, D.; Giordano, C.; Antonietti, M., Sponge-like nickel and nickel nitride structures for catalytic applications. *Advanced Materials (Deerfield Beach, Fla.)* **2013,** *26* (8), 1272-1276.

24. Wienhöfer, G.; Sorribes, I.; Boddien, A.; Westerhaus, F.; Junge, K.; Junge, H.; Llusar, R.; Beller, M., General and selective iron-catalyzed transfer hydrogenation of nitroarenes without base. *Journal of the American chemical society* **2011,** *133* (32), 12875-12879.

25. Zhou, P.; Zhang, Z., One-pot Reductive Amination of carbonyl Compounds with Nitro Compounds by Transfer Hydrogenation over Co–Nx as catalyst. *ChemSusChem* **2017,** *10* (9), 1892-1897.

26. Zhou, P.; Zhang, Z.; Jiang, L.; Yu, C.; Lv, K.; Sun, J.; Wang, S., A versatile cobalt catalyst for the reductive amination of carbonyl compounds with nitro compounds by transfer hydrogenation. *Applied Catalysis B: Environmental* **2017,** *210*, 522-532.

27. Li, M.; Hao, Y.; Cárdenas-Lizana, F.; Yiu, H. H.; Keane, M. A., "Hydrogen-Free"Hydrogenation of Nitrobenzene Over Cu/SiO 2 Via Coupling with 2-Butanol Dehydrogenation. *Topics in Catalysis* **2015,** *58*, 149-158.

28. Long, J.; Zhou, Y.; Li, Y., Transfer hydrogenation of unsaturated bonds in the absence of base additives catalyzed by a cobalt-based heterogeneous catalyst. *Chemical Communications* **2015,** *51* (12), 2331-2334.

29. Huang, Y.; Xie, L.; Zhuo, K.; Zhou, H.; Zhang, Y., Simultaneous catalytic reduction of p-nitrophenol and hydrogen production on MIL-101 (Fe)-based composites. *New Journal of Chemistry* **2021,** *45* (6), 3120-3127.

30. Ma, Y.; Chi, B.; Liu, W.; Cao, L.; Lin, Y.; Zhang, X.; Ye, X.; Wei, S.; Lu, J., Tailoring of the proximity of platinum single atoms on CeO2 using phosphorus boosts the hydrogenation activity. *Acs Catalysis* **2019,** *9* (9), 8404-8412.

31. Li, Y.; Zhou, Y.-X.; Ma, X.; Jiang, H.-L., A metal–organic framework-templated synthesis of γ-Fe 2 O 3 nanoparticles encapsulated in porous carbon for efficient and chemoselective hydrogenation of nitro compounds. *Chemical Communications* **2016,** *52* (22), 4199-4202.

32. Tian, M.; Cui, X.; Liang, K.; Ma, J.; Dong, Z., Efficient and chemoselective hydrogenation of nitroarenes by γ-Fe 2 O 3 modified hollow mesoporous carbon microspheres. *Inorganic Chemistry Frontiers* **2016,** *3* (10), 1332-1340.

33. Cui, X.; Zhang, Q.; Tian, M.; Dong, Z., Facile fabrication of γ-Fe 2 O 3-nanoparticle modified N-doped porous carbon materials for the efficient hydrogenation of nitroaromatic compounds. *New Journal of Chemistry* **2017,** *41* (18), 10165-10173.

34. Nasrollahzadeh, M.; Nezafat, Z.; Gorab, M. G.; Sajjadi, M., Recent progresses in graphene-based (photo) catalysts for reduction of nitro compounds. *Molecular Catalysis* **2020,** *484*, 110758.

35. Xiao, Q.; Sarina, S.; Waclawik, E. R.; Jia, J.; Chang, J.; Riches, J. D.; Wu, H.; Zheng, Z.; Zhu, H., Alloying gold with copper makes for a highly selective visible-light photocatalyst for the reduction of nitroaromatics to anilines. *ACS Catalysis* **2016,** *6* (3), 1744-1753.

36. Tong, F.; Liang, X.; Ma, F.; Bao, X.; Wang, Z.; Liu, Y.; Wang, P.; Cheng, H.; Dai, Y.; Huang, B., Plasmon-mediated nitrobenzene hydrogenation with formate as the hydrogen donor studied at a single-particle level. *ACS Catalysis* **2021,** *11* (7), 3801-3809.

37. Tan, Y.; Liu, X. Y.; Zhang, L.; Wang, A.; Li, L.; Pan, X.; Miao, S.; Haruta, M.; Wei, H.; Wang, H., ZnAl-hydrotalcite-supported Au25 nanoclusters as precatalysts for chemoselective hydrogenation of 3-nitrostyrene. *Angewandte Chemie* **2017,** *129* (10), 2753-2757.

38. He, Z.; Dong, B.; Wang, W.; Yang, G.; Cao, Y.; Wang, H.; Yang, Y.; Wang, Q.; Peng, F.; Yu, H., Elucidating interaction between palladium and N-doped carbon nanotubes: effect of electronic property on activity for nitrobenzene hydrogenation. *ACS Catalysis* **2019,** *9* (4), 2893-2901.

39. Daems, N.; Risplendi, F.; Baert, K.; Hubin, A.; Vankelecom, I. F.; Cicero, G.; Pescarmona, P. P., Doped ordered mesoporous carbons as novel, selective electrocatalysts for the reduction of nitrobenzene to aniline. *Journal of Materials Chemistry A* **2018,** *6* (27), 13397-13411.

40. Akhade, S. A.; Singh, N.; Gutiérrez, O. Y.; Lopez-Ruiz, J.; Wang, H.; Holladay, J. D.; Liu, Y.; Karkamkar, A.; Weber, R. S.; Padmaperuma, A. B., Electrocatalytic hydrogenation of biomass-derived organics: a review. *Chemical reviews* **2020,** *120* (20), 11370-11419.

41. Jin, M.; Liu, Y.; Zhang, X.; Wang, J.; Zhang, S.; Wang, G.; Zhang, Y.; Yin, H.; Zhang, H.; Zhao, H., Selective electrocatalytic hydrogenation of nitrobenzene over copper-platinum alloying catalysts: Experimental and theoretical studies. *Applied Catalysis B: Environmental* **2021,** *298*, 120545.

42. Zhang, W.; Zhang, W.; Tan, J.; Pan, D.; Tang, Y.; Gao, Q., Alloying promotion of Pd-based metallenes in electrocatalytic hydrogenation of functionalized nitroarenes. *Journal of Materials Chemistry A* **2023,** *11* (14), 7505-7512.

43. Liu, M.; Kong, A.; Zhang, J.; Fu, Y.; Li, W., Phytic acid-assisted fabrication of superhydrophilic Ru 3D electrode for electrocatalytic hydrogenation of p-Nitrophenol. *International Journal of Hydrogen Energy* **2022,** *47* (4), 2187-2199.

44. Serrà i Ramos, A.; Alcobé i Ollé, X.; Sort, J.; Nogués, J.; Vallés Giménez, E., Highly efficient electrochemical and chemical hydrogenation of 4-nitrophenol using recyclable narrow mesoporous magnetic CoPt nanowires. *Journal of Materials Chemistry A, 2016, vol. 4, p. 15676-15687* **2016**.

45. Liu, P.; Qin, R.; Fu, G.; Zheng, N., Surface Coordination Chemistry of Metal Nanomaterials. *Journal of the American Chemical Society* **2017,** *139* (6), 2122-2131.

46. Bell, A. T., The impact of nanoscience on heterogeneous catalysis. *Science* **2003,** *299* (5613), 1688-1691.

47. Chen, Y.; Ge, X.; Cao, Y.; Yao, C.; Zhang, J.; Qian, G.; Zhou, X.; Duan, X., Size dependence of Pd-catalyzed hydrogenation of 2, 6-diamino-3, 5-dinitropyridine. *Industrial & Engineering Chemistry Research* **2022,** *61* (19), 6427-6435.

48. Huang, X.; Li, Y.; Li, Y.; Zhou, H.; Duan, X.; Huang, Y., Synthesis of PtPd Bimetal Nanocrystals with Controllable Shape, Composition, and Their Tunable Catalytic Properties. *Nano Letters* **2012,** *12* (8), 4265-4270.

49. Serna, P.; Concepcion, P.; Corma, A., Design of highly active and chemoselective bimetallic gold–platinum hydrogenation catalysts through kinetic and isotopic studies. *Journal of Catalysis* **2009,** *265* (1), 19-25.

50. Huang, Z. F.; Wang, J.; Peng, Y.; Jung, C. Y.; Fisher, A.; Wang, X., Design of efficient bifunctional oxygen reduction/evolution electrocatalyst: recent advances and perspectives. *Advanced Energy Materials* **2017,** *7* (23), 1700544.

51. Bu, L.; Zhang, N.; Guo, S.; Zhang, X.; Li, J.; Yao, J.; Wu, T.; Lu, G.; Ma, J.-Y.; Su, D.; Huang, X., Biaxially strained PtPb/Pt core/shell nanoplate boosts oxygen reduction catalysis. *Science* **2016,** *354* (6318), 1410-1414.

52. Huang, H.; Jia, H.; Liu, Z.; Gao, P.; Zhao, J.; Luo, Z.; Yang, J.; Zeng, J., Understanding of Strain Effects in the Electrochemical Reduction of CO2: Using Pd Nanostructures as an Ideal Platform. *Angewandte Chemie International Edition* **2017,** *56* (13), 3594-3598.

53. Wu, J.; Qi, L.; You, H.; Gross, A.; Li, J.; Yang, H., Icosahedral Platinum Alloy Nanocrystals with Enhanced Electrocatalytic Activities. *Journal of the American Chemical Society* **2012,** *134* (29), 11880-11883.

54. Mao, Y.; Elsherbeni, A. Z.; Jiang, T.; Li, S., Mixed surface impedance boundary condition for FDTD simulations. *IET Microwaves, Antennas & Propagation* **2017,** *11* (9), 1197-1202.

55. Boronat, M.; Concepción, P.; Corma, A.; González, S.; Illas, F.; Serna, P., A Molecular Mechanism for the Chemoselective Hydrogenation of Substituted Nitroaromatics with Nanoparticles of Gold on TiO2 Catalysts: A Cooperative Effect between Gold and the Support. *Journal of the American Chemical Society* **2007,** *129* (51), 16230-16237.

56. Makosch, M.; Sá, J.; Kartusch, C.; Richner, G.; van Bokhoven, J. A.; Hungerbühler, K., Hydrogenation of Nitrobenzene Over Au/MeO Catalysts—A Matter of the Support. *ChemCatChem* **2012,** *4* (1), 59-63.

57. Westerhaus, F. A.; Jagadeesh, R. V.; Wienhöfer, G.; Pohl, M.-M.; Radnik, J.; Surkus, A.-E.; Rabeah, J.; Junge, K.; Junge, H.; Nielsen, M.; Brückner, A.; Beller, M., Heterogenized cobalt oxide catalysts for nitroarene reduction by pyrolysis of molecularly defined complexes. *Nature Chemistry* **2013,** *5* (6), 537-543.

58. Jia, R.; Wang, Y.; Wang, C.; Ling, Y.; Yu, Y.; Zhang, B., Boosting selective nitrate electroreduction to ammonium by constructing oxygen vacancies in TiO2. *Acs Catalysis* **2020,** *10* (6), 3533-3540.

59. Zhang, Y.-F.; Mellah, M., Convenient electrocatalytic synthesis of azobenzenes from nitroaromatic derivatives using SmI2. *ACS Catalysis* **2017,** *7* (12), 8480-8486.

60. Gelder, E. A.; Jackson, S. D.; Lok, C. M., The hydrogenation of nitrobenzene to aniline: a new mechanism. *Chemical communications* **2005,** (4), 522-524.

61. Cui, Q. H.; Jiang, L.; Zhang, C.; Zhao, Y. S.; Hu, W.; Yao, J., Coaxial Organic p-n Heterojunction Nanowire Arrays: One-Step Synthesis and Photoelectric Properties. *Advanced Materials* **2012,** *24* (17), 2332-2336.

62. Mahata, A.; Rai, R. K.; Choudhuri, I.; Singh, S. K.; Pathak, B., Direct vs. indirect pathway for nitrobenzene reduction reaction on a Ni catalyst surface: a density functional study. *Physical Chemistry Chemical Physics* **2014,** *16* (47), 26365-26374.

63. Wang, S.; Liu, Y.; Zhao, J., PtN 3-Embedded graphene as an efficient catalyst for electrochemical reduction of nitrobenzene to aniline: a theoretical study. *Physical Chemistry Chemical Physics* **2020,** *22* (31), 17639-17645.

Chapter 2

Selective Electrocatalytic Hydrogenation of 3-NS to 3-VA on Pd- and Pt- based Nanomaterials

2.1 Background and motivation

Hydrogenation of nitroaromatics to aniline derivatives is a crucial process in the production of pharmaceuticals, dyes, fragrances, and other chemicals. Since 2020, global annual aniline production has exceeded 6 million tons. Currently, most industrial aniline production involves direct redox reactions using stoichiometric reducing agents, such as iron in acidic media or tin chloride, to reduce nitroaromatics. However, this process has low selectivity (<50%) and generates large amounts of metal-ion-containing wastewater, irreversible environmental hazards.

In recent years, rapid advancements in thermal catalysis have led to extensive research into using this method for nitroaromatics hydrogenation. Metals like Pt, Pd, Au, and Ag have shown high selectivity for aniline production (>90%). Typically, these thermal catalytic reactions occur under high-pressure hydrogen and high-temperature conditions, making the reaction pathways difficult to control and introducing significant safety risks. Additionally, the hydrogen required for these reactions is primarily sourced from methane reforming. The reliance on high-performance catalysts, particularly noble metals, results in high costs and increased carbon emissions.

ECH offers a sustainable alternative for hydrogenating unsaturated functional groups by using renewable electricity as the energy source and water as the hydrogen source. This method operates under mild conditions[1-4], avoiding the harsh operational conditions associated with high temperatures and H_2 pressures, making it more aligned with current sustainability goals. ECH provides a controlled alternative for multi-electron transfer processes by conveniently and accurately adjusting the potential or current at the working electrode, enabling precise control over the reaction[5-7]. The advantages of ECH make it a promising approach for selective hydrogenation reactions, contributing to environmentally friendly and sustainable chemical processes.

3-NS is primarily derived from the industrial production of styrene. It consists of a styrene molecule with a nitro group attached to the third carbon on the benzene ring. At room temperature, it appears as a pale-yellow liquid. By selectively hydrogenating 3-NS, it can be reduced to 3-VA (only $-NO_2$ reduced). Other possible product include: 3-EN (only -C=C reduced), 3-EA (both $-NO_2$ and -C=C reduced).

Well-designed electrocatalysts play a crucial role in facilitating efficient conversion through target pathways. Metals like platinum (Pt) and palladium(Pd) exhibit high activity in thermal catalytic hydrogenation reactions[8]. Therefore, we began by exploring commercial Pt and Pd catalysts to identify suitable reaction conditions for the ECH of 3-NS. Our hypothesis is that Pt and Pd's strong adsorption capabilities often lead to the co-reduction of the vinyl group to an ethyl group during the nitro-reduction process, resulting in lower selectivity of the desired product. To address this, we hypothesize that the synergistic effects of alloying with different transition metals can reduce the adsorption strength of platinum group metal atoms on intermediates, thereby enhancing selectivity. Alloying not only improves catalytic properties but also reduces the consumption of precious metals.

This study successfully achieved the highly selective electrocatalytic reduction of 3-NS for the first time. By leveraging the alloying effect, catalysts such as CuPd, CoPt, and Co_2P/Pt were designed and synthesized. These catalysts enabled the chemoselective hydrogenation of 3-NS to the valuable product 3-VA over a wide potential range of -0.05V to 0.45V vs. RHE. At -0.45V vs. RHE, the selectivity for 3-VA exceeded 80.0%, outperforming commercial Pd/C and Pt/C catalysts (<40 %). The alloying effect's promotion of selectivity and efficiency was preliminarily validated through experimental studies.

2.2 Experiment

2.2.1 Materials

Poly(vinylidene fluoride) (PVDF), n-Methyl-2-pyrrolidone (NMP, 99%), and hydrazine monohydrate (>99%) were purchased from Alfa Aesar. Dicobalt octacarbonyl ($Co_2(CO)_8$, 95%) and Copper(I) chloride (CuCl, 97%) were purchased from Strem Chemicals. Oleic acid (OAc, 90%), 1,2-dichlorobezene (99%), 1-octadecene (ODE 90%), $Pt(acac)_2$(98%), Tri-n-butyl Phosphate (TBP, > 99%), Trioctylphosphine oxide (TOPO, >99%) were purchased from Acros Organics. 3-VA (>99%), benzyl ether and oleylamine (OLAM, 70%) were purchased from Sigma Aldrich. 3-NS (97%), 3-EA (99%) were purchased from Thermo Scientific. 3-EN (99%) was purchased from Ambeed. Vulcan carbon (XC-72R), carbon paper (Toray paper 060) and proton exchange membrane (PFSA D170-U) used in the electrochemical cell were purchased from Fuel Cell Store. All the materials were used without further purification.

2.2.2 Pd- and Pt- based nanomaterials preparation

CuPd synthesis

0.149 g of CuCl, 0.81g of $PdBr_2$ and 18 mL of OLAM were vacuumed in a three-necked flask by vigorous stirring at 90 °C for 60 min. Under N_2 protection, the solution was heated up to 230 °C at 10 °C/min after 0.2 mL TBP injected. Then the solution was refluxed for 2 h before it was cooled down to room temperature. The product was collected by centrifugation at 8000 rpm after the addition of 45 mL of hexanes. Then, the CuPd alloy was purified twice by centrifugation in 40 mL of isopropanol and 5 mL of hexane. The collected CuPd was re-dispersed and stored in hexanes for further use.

CoPt synthesis

0.064 g of $Pt(acac)_2$ was dissolved in 10 mL OLAM and 5 mL benzyl ether, in the presence of 0.242 g 1-tetradecanediol, 0.505 g 1-adamantanecarboxylic acid. The formed solution was heated to 200 °C under Ar flow. 0.086 g of cobalt carbonyl dissolved in 1 mL of dichlorobenzene was added into this hot solution under the Ar atmosphere. After 30 minutes, the solution temperature was raised to 260 °C and kept in reflux for 30 minutes. After the reaction, the solution was cooled down to room temperature. 40 mL iso-propanol and 20 mL ethanol were added to precipitate NPs, followed by centrifuge (6500 rpm, 6 minutes). The collected CoPt was re-dispersed and stored in hexane for further use.

$CoPt_3$ synthesis

0.266 g of $Pt(acac)_2$ was dissolved in a solution of 41 mL of OLAM and 16 mL of ODE. The reaction mixture was kept at 80 °C for 30 min under vacuum and then heated to 300 °C under N_2 atmosphere. 0.103 g of $Co_2(CO)_8$ was dissolved in 3.2 mL of 1,2-dichlorobezene and injected into the reaction mixture at 170 °C. The reaction mixture was heated to 300 °C at a rate of 10 °C/min. After 30 min, the reaction mixture was cooled to room temperature. The resulting $CoPt_3$ as re-dispersed and stored in hexane for further use.

Co_2P nanorods (NRs) synthesis

2 g of $Co(acac)_2 \cdot 4H_2O$, 3.2 g of TOPO, 80 mL of benzyl ether, and 8 mL of OAc, were added to a reactor flask with a Teflon coated magnetic stir bar. The solution was stirred and heated to 140 ºC while being purged with N_2 for one hour. The solution was then cooled to 100 ºC and put under vacuum to degas and remove moisture for one hour. The reaction was then switched to N_2 and heated to 220 ºC at a heating rate of 5 ºC/min. Once at 220 ºC, 12 mL of TBP was injected via syringe. The solution was then heated to 260ºC at a heating rate of 5 ºC/min and aged for two hours. The solution was then cooled to room temperature and the NRs were separated via centrifugation (8000 rpm, 8 min) under an inert atmosphere with distilled isopropanol. The NRs were further washed by 2-3 cycles of dispersion (using distilled hexanes) and precipitation (using distilled isopropanol). The Co_2P NRs were stored in hexanes in under inert atmosphere for future use.

Co_2P/Pt nanorods NRs synthesis

12.5 mg of $Pt(acac)_2$ was dissolved in 6 mL of ODE, 1 mL of OLAM, and 0.5 mL of OAc, in a reactor flask with a Teflon coated magnetic stir bar. The solution was stirred and heated to 100ºC under vacuum for 1 hour to degas and remove moisture. The reaction was switched to N_2, and 17.5 mg of seed was injected. Using a syringe pump, the reducing solution (1 mL of OLAM, 2 mL of ODE, and 12 mg of BTBA) was injected at a rate of 0.3 mL/min. The solution was then heated to 180 ºC at a heating rate of 3 ºC/min and aged for 30 min. The NRs were separated via centrifugation (8000 rpm, 8 min) with isopropanol. The NRs were further washed by 2-3 cycles of dispersion using hexanes and precipitation using isopropanol. The NRs were redispersed and stored in hexanes.

2.2.3 Preparation of carbon supported electrodes

40 mg of carbon black (Vulcan XC 72R) was dispersed in 10 mL of hexanes and sonicated for 1 hour. Then, 20 wt.% of the prepared metal nanocrystals (dispersed in hexanes) was added dropwise to the carbon black suspension and sonicated for another hour. The supported nanocrystals were collected by centrifugation at 8000 rpm for 8 minutes. To remove surfactants attached to the nanomaterial surfaces, the catalysts were stirred overnight in a 1% v/v hydrazine/ethanol solution, then washed three times by centrifugation at 10000 rpm for 10 minutes, each time with the addition of 25 mL of ethanol. Finally, the catalysts were dried under vacuum. The metal mass loading amount for the carbon-supported catalysts was confirmed by ICP-OES. A measured amount of dried catalyst, along with 10 wt. % of PVDF and 500 μL of NMP, was thoroughly mixed, and the mixture was applied onto carbon paper (total area 1 cm^2). The metal loading on the carbon paper was maintained at 0.3 mg cm^{-2} for all Pd or Pt components in the carbon-supported catalysts.

2.2.4 Catalyst characterization set-up

XRD measurements were performed using an Empyrean Multipurpose X-ray diffractometer equipped with Cu Kα radiation (λ = 0.15406 nm) at 40 kV and 30 mA, employing a scan of 0.05°s^{-1} from 20° to 90°. TEM images were obtained on a FEI Tecnai Spirit (120 kV). Inductively coupled plasma optical emission spectrometry (ICP-OES) analyses were conducted on a PerkinElmer Avio-200 ICP optical emission spectrometer to determine the metal loading on the carbon supported Cu NCs.

2.2.5 Catalytic performance set-up

All electrocatalytic studies were performed at room temperature in 0.1 M $LiClO_4$ and 5 mM 3-NS dissolved in distilled water and ethanol (v_1: v_2=1:1 (~pH=6.80), using an Autolab Potentiostat (PGSTAT128N, Metrohm AG), The catalysts were loaded onto a carbon paper (1 cm × 1 cm) as working electrode. An Ag/AgCl (4.0 M KCl) was as reference electrode, and a Pt gauze was as counter electrode. All reaction were reacted for 3 hours to avoid crossover error. All potentials (E) were reported *vs*. RHE according to the following equation:

$$E\ (vs.\ \text{RHE}) = E\ (vs.\ \text{Ag/AgCl}) + 0.62\ V$$

where 0.62 V is the potential difference between the Ag/AgCl reference electrode and hydrogen reference electrode in 0.1 M $LiClO_4$ and 5 mM 3-NS electrolyte solution, which was calibrated by the open circuit potential test before the electrochemical measurement.

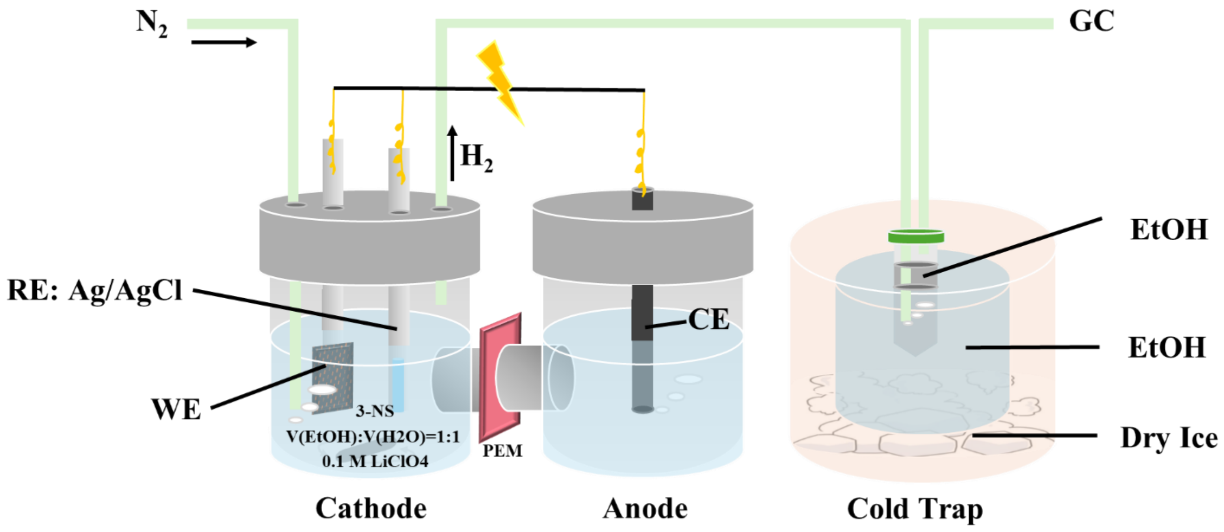

Figure 2.1 Schematic figure of the H-cell set-up.

During the electrolysis, N_2 was steadily supplied to the cathode compartment of H-Cell (**Figure 2.1**) at a rate of 5 sccm, and the gas phase effluent in the headspace of the cathode compartment was continuously introduced to a cold trap filled with CH_3CN at -20 °C before it entered the sampling loop of a gas chromatograph and being analyzed by GC (Shimadzu, GC2014) (**Figure 2.2**). The liquid phase products from both the cold trap and the H cell were analyzed using a high-performance liquid chromatograph (Shimadzu, LC20-AD) equipped with a C18 column (Luna Omega, Phenomenex) and a photodiode array (PDA) UV-Vis detector (Shimadzu, SPD-M20A) at 275 nm for all products (**Figure 2.3**).

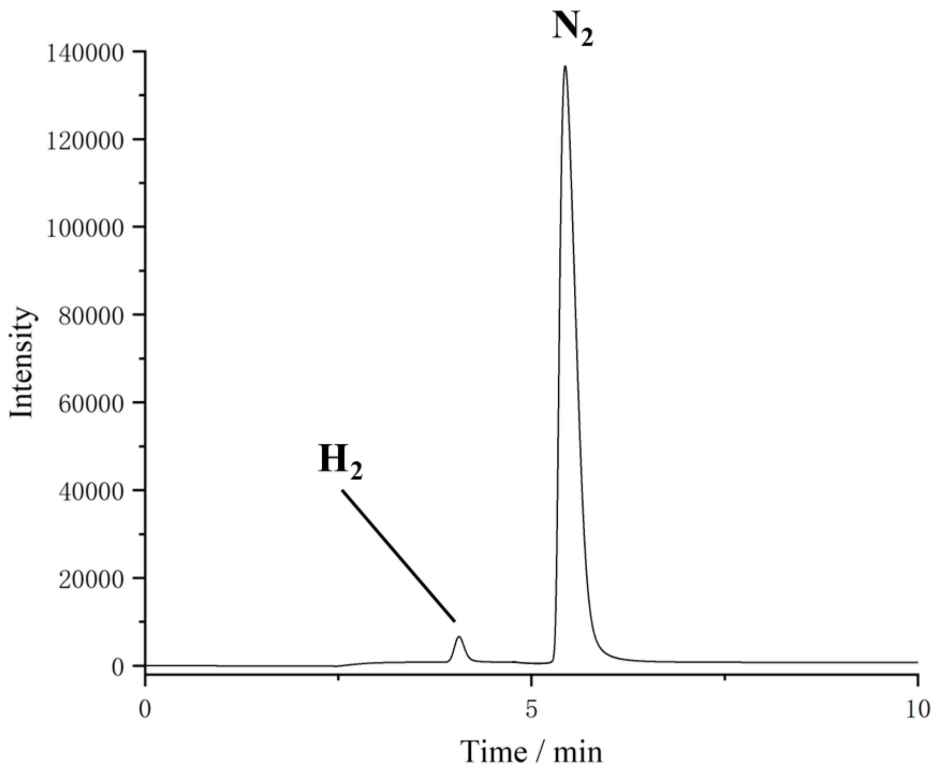

Figure 2.2 Typical GC-TCD chromatogram of the gaseous products.

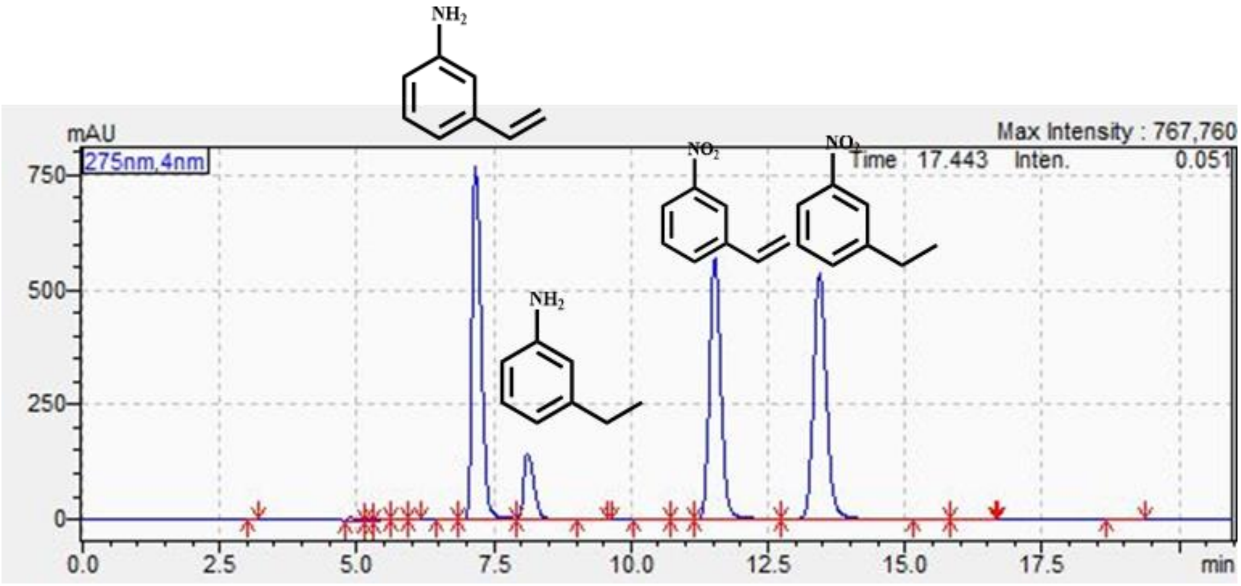

Figure 2.3 Typical HPLC PDA chromatogram of the liquid products in H-cell at 275 nm.

2.2.6 Calculations of faradaic efficiency

Faradaic efficiency to liquid product i (i = 3-VA, 3-EA, 3-EN) were calculated by:

$$FE_i = N_i Z_i FQ \text{ x } 100\ \%$$

where N_i is the number of moles of product i, Zi is the number of electrons transferred per molecule of product (6 for 3-VA, 8 for 3-EA, 2 for 3-EN), F is the Faraday constant (96485.3 C mol-1), and Q is the total charge passed through the system.

The incremental amount of evolved H_2 (N_{H2}, moles) was calculated by:

$$N_{H2} = C_{H2} \text{ x } 10^{-3} \times PVRT \times 100\ \%$$

where C_{H2} is the concentration (ppth) of H_2 measured by GC, P is the atmospheric pressure (1.013×10^5 Pa), R is the gas constant (8.314 $J \cdot mol^{-1} \cdot K^{-1}$), T is the absolute temperature (293 K).

The instantaneous faradaic efficiency of H_2 (fe_{H2}) was calculated by:

$$fe_{H2} = N_{H2} Z_{H2} F \Delta Q \times 100\ \%$$

where Z_{H2} is the number of electrons transferred per molecule of H_2, ΔQ is the incremental charge transferred during the time (t) required to fill the sampling loop. The time was determined as: $t = V/\text{flow rate} = 1\ cm^3 / 10\ cm^3/min \times 60\ s/ 1\ min =$

6 s. Overall faradaic efficiency to H_2 (FE_{H2}) was determined as the average of fe_{H2} values measured throughout the reaction.

2.3 Results and discussion

2.3.1 Sructural characterization of Pd- and Pt- based catalysts

To understand the role of different intermetallics in the reduction of 3-NS from a bottom-up perspective, we synthesized various Pd- and Pt- based nanomaterials for study. **Figure 2.4 (a)** shows the XRD pattern of CuPd compared with ICSD database data. The primary diffraction lines at 2θ values of approximately 43.4°, 62.6°, and 78.8° correspond to the (110), (200), and (211) planes of CuPd, respectively, indicating that all CuPd is in a metallic state and not oxidized. **Figure 2.4 (b)** shows the XRD pattern of CoPt. The primary diffraction lines at 2θ values of approximately 32.1°, 42.3°, 48.7°, and 70.6° correspond to the (110), (111), (200), and (220) planes of CoPt. **Figures 2.5 (a)** and **2.9 (a)** show the morphological characterization of. **Figures 2.5 (a)-(f)** display TEM images of commercial Pd/C, commercial Pt/C, CuPd, CoPt/C, Co_2P and Co_2P/Pt nanomaterials. More structural characterization data still need to be completed in the upcoming stages.

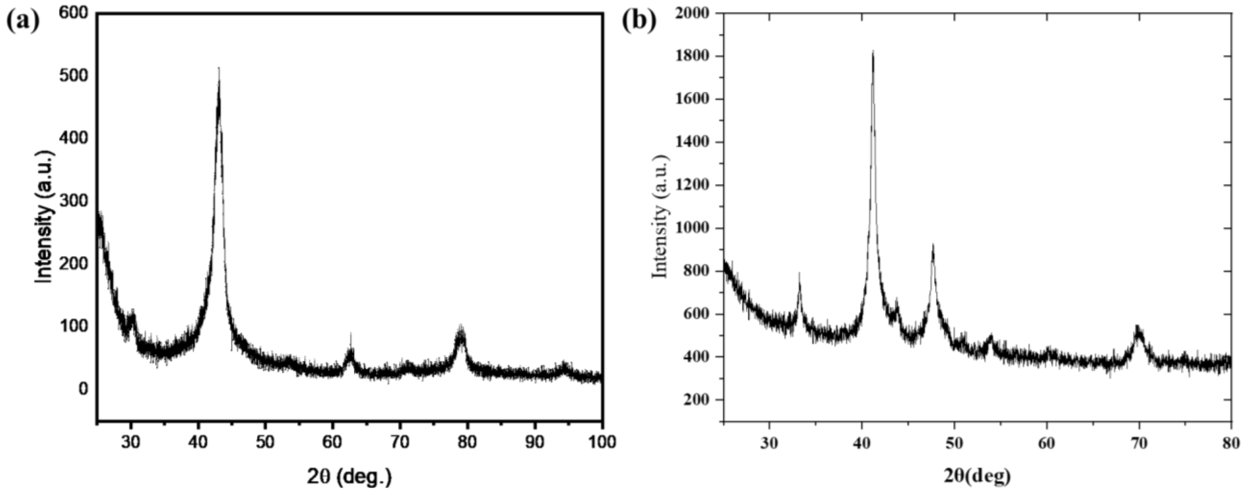

Figure 2.4 XRD patterns of **(a)** CuPd, **(b)** CoPt.

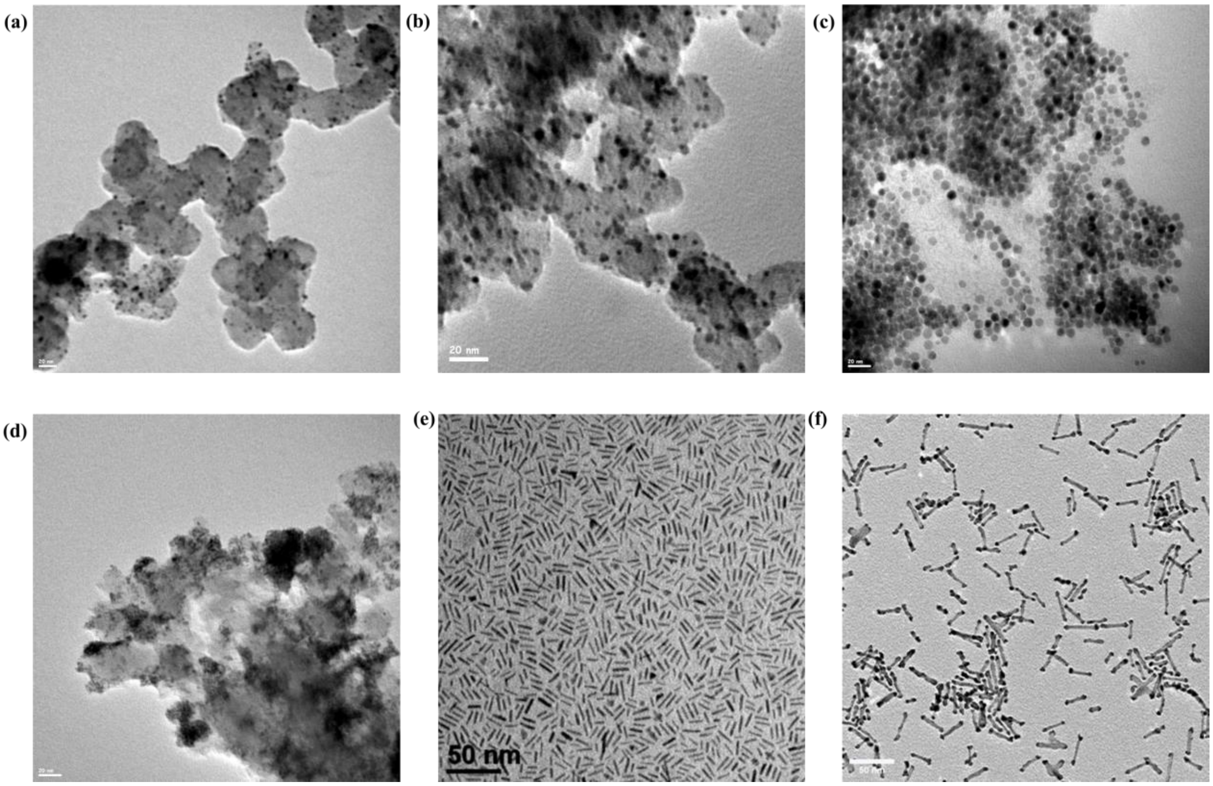

Figure 2.5 TEM image of **(a)** commercial Pd/C catalyst; **(b)** commercial Pt/C catalyst; **(c)** CuPd; **(d)** CoPt/C; **(e)** Co_2/P; **(f)** Co_2P/Pt.

2.3.2 Electrochemical performance for 3-NS electrocatalytic hydrogenation

Before conducting electrocatalysis tests, catalysts were electrochemically cleaned through repeated CV cycles. A significant increase in current density indicated the successful removal of adsorbed surfactants. The cathodic reduction of 3-NS prior to HER confirmed its thermodynamic preference, where electrons reduce nitroaromatics either through chemisorbed H* or via proton-coupled electron transfer (PCET) processes[9, 10]. The selective hydrogenation of nitro and vinyl groups in 3-NS produces 3-VA and 3-ethyl nitrobenzene (3-EN), which can further reduce to 3-EA[11]. Since the reducing the nitro group is thermodynamically more favorable than reducing the vinyl group, the formation of 3-EN is generally suppressed.

Electrocatalysis tests were conducted in a solution of 0.1 M LiClO4 containing 50 wt % ethanol, for 3 hours at -0.15 to -0.45 V vs. RHE, to enhance the solubility of 3-NS (5 mM). HPLC clearly showed the conversion of 3-NS into the target product 3-VA, along with the byproduct 3-EA and 3-EN.

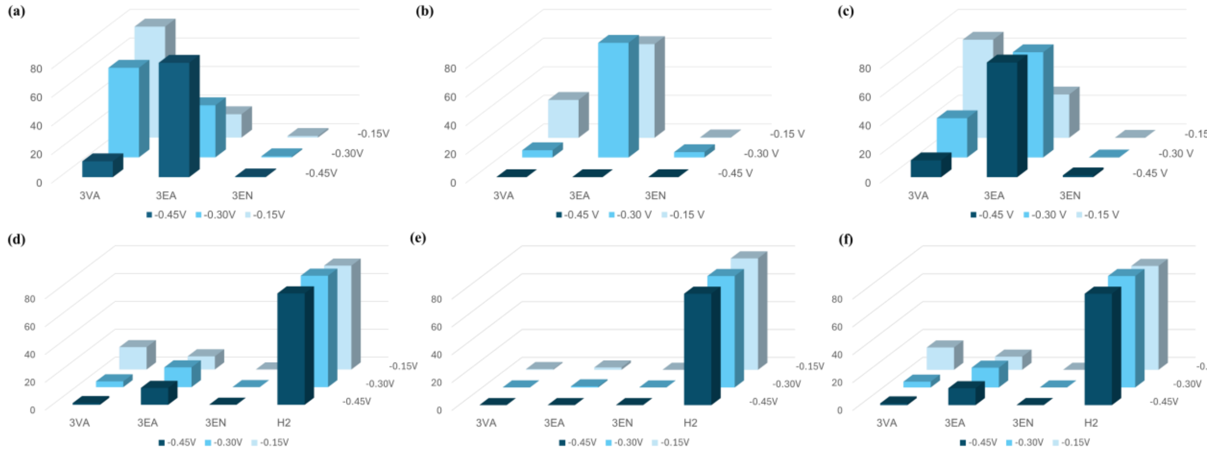

Figure 2.6 Selectivity plots of 3-VA, 3-EA and 3-EN **(a)** in pH=7; **(b)** in pH=1; **(c)** in pH=13 with different voltage applied on commercial Pd/C catalyst; FEs of products for the ECH of 3-NS **(d)** in pH=7; **(e)** in pH=1; **(f)** in pH=13 with different voltage applied on commercial Pd/C catalysts.

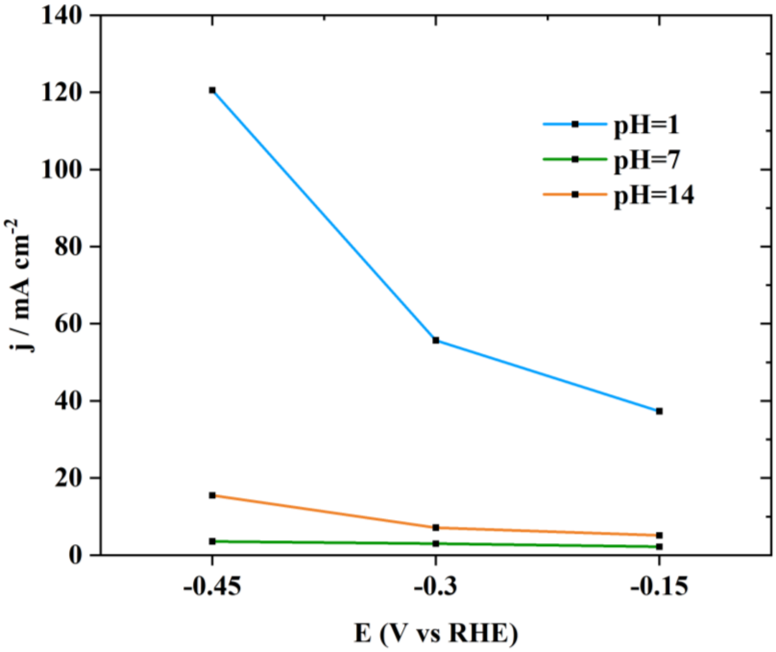

Figure 2.7 Current density plot of 3-NS in different pH and voltage applied on commercial Pd/C catalyst.

Commercial catalysts

Since this is the first electrocatalytic reduction test for 3-NS, we initially used commercial catalysts. Based on thermocatalytic experiments and the electroreduction of nitrobenzene, we used commercial Pt/C and Pd/C catalysts[12]. As shown in **Figure 2.7**, experiments under different pH conditions indicated that acidic and basic environments produced higher currents than neutral conditions, with current density decreasing as more positive overpotentials were applied. This is mainly because the slow water dissociation step requires higher overpotentials to drive the reaction. However, regarding product selectivity, as shown in **Figure 2.6 (a)-(c)**, neutral conditions achieved higher selectivity at the same potential, with more positive potentials led to higher selectivity under the same conditions. Due to the strong HER in acidic condition, a lot of bubbles generate, and the most reactants and products are brought out to the cold trap without involving the reaction. At more negative potentials (e.g., -0.30 and -0.45 V vs. RHE), the FE for 3-VA decreased significantly due to over-hydrogenation of the vinyl group, as shown in **Figure 2.8 (d)-(f)**. This suggests that more negative potentials favor the hydrogenation of the vinyl group in 3-VA, where the reduction of nitro or vinyl groups is less favorable than the release of H_2. Notably, the ECH pathway may be able to controlled by simply adjusting the working potential[13]. However, from an industrial perspective, to produce more valuable 3-VA on a large scale, electrolysis should be performed at potentials above -0.45 V vs. RHE. Controlling the over-hydrogenation of the vinyl group and reducing competitive HER is a major challenge. For commercial Pt/C catalysts (**Figure 2.8 (a)**), the electroreduction of 3-NS to 3-VA achieved higher selectivity over a wide potential range compared to Pd/C (**Figure 2.6(a)**). At a potential of -0.15 V vs. RHE, selectivity was close to 80% on commercial Pt/C catalysts. However, due to its higher activity for HER compared to commercial Pd/C, the faradaic efficiency for the electroreduction of 3-NS was lower.

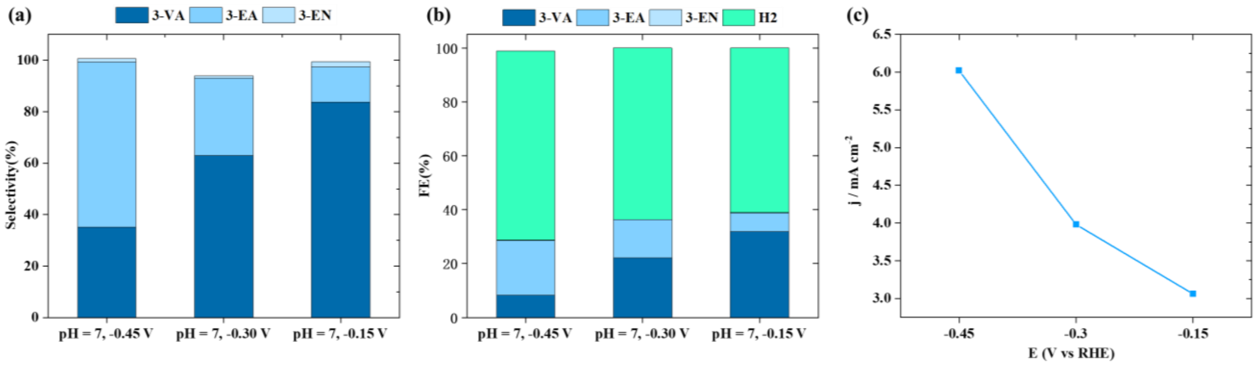

Figure 2.8 (a) selectivity plots of 3-VA, 3-EA and 3-EN with different voltage applied on commercial Pt/C catalyst; **(b)** FEs of products for the ECH of 3-NS over commercial Pt/C catalyst in a wide potential range of −0.05 to −0.45 V *vs.* RHE (3-NS: 5 mM, reaction time: 3 h); **(c)** current density plot of 3-NS with different voltage applied.

Synthesized catalysts

In order to enhance the selectivity of 3-NS to 3-VA and reduce the HER reaction, based on the alloy effect we mentioned in **Section 1.3**, we synthesized CuPd, CoPt, and $CoPt_3$. Compared to commercial Pd/C catalysts, CuPd significantly improved the selectivity for 3-VA (**Figure 2.10(a)**), from 10% to over 50%, indicating that the incorporation of Cu enhances the activity of the reaction sites for 3-NS reduction. The cobalt-platinum alloys showed better activity than the single metals Co (~ 40%)

and Pt(< 40%). CoPt achieved higher selectivity than $CoPt_3$ (**Figure 2.9 (b)**). We hypothesize that the doping of Co and Cu reduces the adsorption of 3-NS ECH reaction intermediates on Pd or Pt atoms, thereby preventing further hydrogenation of 3-VA and increasing its selectivity.

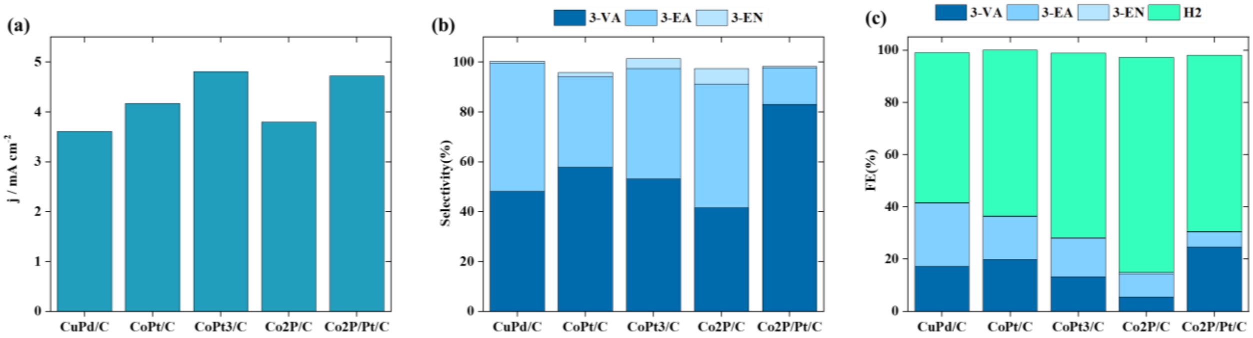

Figure 2.9 (a) current density plot of 3-NS in -0.45V vs RHE, pH=6.8 over different catalysts; **(b)** selectivity of 3-NS ECH over different catalysts; **(c)** FEs of products for the ECH of 3-NS over different catalysts in −0.45 V vs. RHE (3-NS: 5 mM, reaction time: 3 h).

We also synthesized Co_2P/Pt based on literature methods[14]. As shown in **Figure 2.10 (b)**, the Co_2P/Pt catalyst improved the selectivity for 3-VA compared to CoPt and commercial Pt/C catalysts. The Co_2P/Pt NRs successfully achieved 83% selectivity, indicating its effectiveness in inhibiting further hydrogenation of 3-VA. However, for all the catalysts we used, HER remains the main factor affecting FE. We found that CuPd showed the most significant reduction in HER among all the alloy catalysts we tested. We hypothesize that this may be due to the doping of Cu, which alters the hydrogen binding energy of Pd, thereby suppressing HER activity. Therefore, in the future, the design strategy of the catalyst for ECH of 3-NS-to-3-VA is to have low adsorption of 3-NS ECH reaction intermediates while also exhibiting low HER activity.

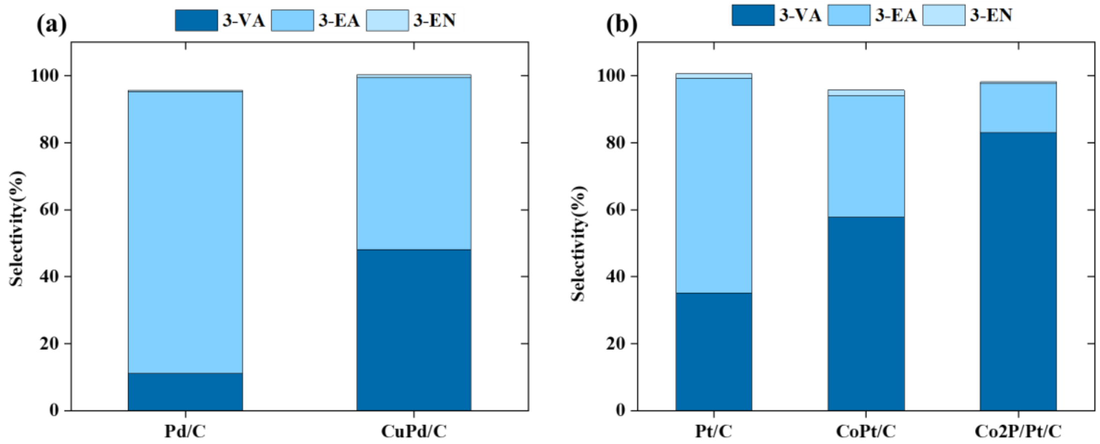

Figure 2.10 (a) comparison of selectivity commercial Pd and CuPd catalyst **(b)** comparison of selectivity over commercial Pt, CoPt and Co_2P/Pt alloy and intermetallic.

2.4 Conclusion

This study demonstrates the effectiveness of electrocatalytic hydrogenation (ECH) as a method for the selective reduction of 3-NS under ambient conditions, utilizing sustainable electricity and water as hydrogen source. Through a series of experiments, we highlighted the superior performance of alloys, particularly Co_2P/Pt, in achieving high selectivity and efficiency for the production of 3-VA. Our findings show that alloying transition metals with Pt group metals can significantly enhances catalytic activity and selectivity, outperforming commercial Pt/C and Pd/C catalysts. The introduction of Cu into Pd-based catalyst, Co into Pt-based catalysts, as well as the optimization of working potentials, also proved crucial in minimizing competing reactions like HER.

While the initial results are promising, further work is necessary to fully understand the structural characteristics, to find out the exact Co-Pt ratio that achieves the best catalytic performance, and other potential excellent catalysts for ECH of 3-NS. Additional structural characterization, including advanced TEM, X-ray photoelectron spectroscopy analyses and others, will provide deeper insights into the morphology and crystallography of the synthesized nanomaterials. Moreover, detailed Co/Pt ratio analysis through techniques like ICP-OES and X-ray adsorption spectroscopy will be crucial in correlating compositional factors with catalytic behavior. This continued investigation will help refine the synthesis process and enhance the practical applications of these catalysts in industrial-scale hydrogenation processes.

2.5 Reference

1. Yang, J.; Qin, H.; Yan, K.; Cheng, X.; Wen, J., Advances in electrochemical hydrogenation since 2010. *Advanced Synthesis & Catalysis* **2021,** *363* (24), 5407-5416.

2. Akhade, S. A.; Singh, N.; Gutiérrez, O. Y.; Lopez-Ruiz, J.; Wang, H.; Holladay, J. D.; Liu, Y.; Karkamkar, A.; Weber, R. S.; Padmaperuma, A. B., Electrocatalytic hydrogenation of biomass-derived organics: a review. *Chemical reviews* **2020,** *120* (20), 11370-11419.

3. Zhang, P.; Sun, L., Electrocatalytic hydrogenation and oxidation in aqueous conditions. *Chinese Journal of Chemistry* **2020,** *38* (9), 996-1004.

4. Huang, B.; Sun, Z.; Sun, G., Recent progress in cathodic reduction-enabled organic electrosynthesis: Trends, challenges, and opportunities. *eScience* **2022,** *2* (3), 243-277.

5. Song, J.; Huang, Z.-F.; Pan, L.; Li, K.; Zhang, X.; Wang, L.; Zou, J.-J., Review on selective hydrogenation of nitroarene by catalytic, photocatalytic and electrocatalytic reactions. *Applied Catalysis B: Environmental* **2018,** *227*, 386-408.

6. Lucas, F. W.; Grim, R. G.; Tacey, S. A.; Downes, C. A.; Hasse, J.; Roman, A. M.; Farberow, C. A.; Schaidle, J. A.; Holewinski, A., Electrochemical routes for the valorization of biomass-derived feedstocks: from chemistry to application. *ACS Energy Letters* **2021,** *6* (4), 1205-1270.

7. Jin, M.; Liu, Y.; Zhang, X.; Wang, J.; Zhang, S.; Wang, G.; Zhang, Y.; Yin, H.; Zhang, H.; Zhao, H., Selective electrocatalytic hydrogenation of nitrobenzene over copper-platinum alloying catalysts: Experimental and theoretical studies. *Applied Catalysis B: Environmental* **2021,** *298*, 120545.

8. Downing, R.; Kunkeler, P.; Van Bekkum, H., Catalytic syntheses of aromatic amines. *Catalysis today* **1997,** *37* (2), 121-136.

9. Koh, K.; Sanyal, U.; Lee, M. S.; Cheng, G.; Song, M.; Glezakou, V. A.; Liu, Y.; Li, D.; Rousseau, R.; Gutiérrez, O. Y., Electrochemically tunable proton-coupled electron transfer in Pd-catalyzed benzaldehyde hydrogenation. *Angewandte Chemie* **2020,** *132* (4), 1517-1521.

10. Jensen, S. C.; Bettis Homan, S.; Weiss, E. A., Photocatalytic conversion of nitrobenzene to aniline through sequential proton-coupled one-electron transfers from a cadmium sulfide quantum dot. *Journal of the American Chemical Society* **2016,** *138* (5), 1591-1600.

11. Ren, Y.; Hao, C.; Chang, Q.; Li, N.; Yang, J.; Hu, S., Solar-accelerated chemoselective hydrogenation of 4-nitrostyrene to 4-vinylaniline with carbon dot-induced Cu over Cu 3 P in the absence of any sacrificial reagent. *Journal of Materials Chemistry A* **2021,** *9* (45), 25374-25380.

12. Macino, M.; Barnes, A. J.; Althahban, S. M.; Qu, R.; Gibson, E. K.; Morgan, D. J.; Freakley, S. J.; Dimitratos, N.; Kiely, C. J.; Gao, X., Tuning of catalytic sites in Pt/TiO2 catalysts for the chemoselective hydrogenation of 3-nitrostyrene. *Nature Catalysis* **2019,** *2* (10), 873-881.

13. Chong, X.; Liu, C.; Huang, Y.; Huang, C.; Zhang, B., Potential-tuned selective electrosynthesis of azoxy-, azo-and amino-aromatics over a CoP nanosheet cathode. *National science review* **2020,** *7* (2), 285-295.

14. Liu, C.; Ma, Z.; Cui, M.; Zhang, Z.; Zhang, X.; Su, D.; Murray, C. B.; Wang, J. X.; Zhang, S., Favorable core/shell interface within Co2P/Pt nanorods for oxygen reduction electrocatalysis. *Nano Letters* **2018,** *18* (12), 7870-7875.

Chapter 3

Supporting Information

3.1 Catalysts Pretreatment

The synthesis of colloidal nanoparticles is achieved by controlling nucleation and growth in a homogeneous solution, allowing for the production of desired colloidal nanoparticles[1]. However, nanoparticles synthesized in solution are often covered with organic surfactants, which make them unsuitable for direct use as catalysts. For example, in the synthesis of Pd-based and Pt-based alloy nanoparticles in organic solutions, oleylamine and/or oleic acid are commonly used to stabilize the nanoparticles and control their size and shape. Although these ligands are indispensable during nanoparticle synthesis, they are detrimental to catalytic activity because they hinder the access of reactant molecules to surface atoms. Therefore, before catalytic reactions, it is necessary to remove the surfactants and clean the surface without altering the particle size or morphology. This process is crucial for the application of colloidal nanoparticles in catalysis. Additionally, due to the influence of storage conditions or other potential drawback, the removal of oxides from the catalyst surface and catalyst activation are required to minimize the impact on experimental results.

3.1.1 Surfactant Removal– Hydrazine Wash

In nanomaterial synthesis, oleylamine and oleic acid are commonly used as surfactants to control the growth, shape, and stability of nanoparticles. Oleylamine, a primary amine with a long hydrocarbon chain, and oleic acid, a carboxylic acid, stabilize nanoparticles by adsorbing onto their surface through their polar functional groups while the hydrophobic tail prevents agglomeration. However, after synthesis, these surfactants can block active sites on the nanoparticles, which reduces their efficacy in applications like catalysis, drug delivery, or energy storage. These surfactants are also used in the synthesis of CuPd, CoPt and Co_2P/Pt.

To remove oleylamine and oleic acid, a hydrazine wash is often applied. The mechanism of surfactant removal via hydrazine involves hydrazine acting as a reducing agent, cleaving the bonds between the nanoparticles and the surfactant molecules. Oleylamine is adsorbed onto the nanoparticle surface via its amine group, forming a weak bond through nitrogen-metal coordination. Hydrazine (N_2H_4) disrupts this interaction by reducing the surface-bound oleylamine, weakening its bond with the nanoparticle and promoting desorption.

For oleic acid, the carboxyl group (-COOH) binds to the nanoparticle surface through a similar coordination interaction with metal ions on the nanoparticle. Hydrazine reduces these metal ions or disrupts the electrostatic interactions, leading to desorption of the oleic acid from the nanoparticle surface. The surfactants are then washed away, leaving a clean nanoparticle surface.

By breaking these bonds, hydrazine effectively removes both oleylamine and oleic acid from the nanoparticle surface, allowing the nanoparticles to regain their full functional capacity for applications where a clean surface is essential. The process helps preserve the nanoparticle's structure and size while eliminating the unwanted surfactant layer.

3.1.2 Electrochemical Pretreatment – Cyclic Voltammetry Scanning Method

3.1.2.1 Cyclic Voltammetry (CV)

Cyclic Voltammetry (CV) is a fundamental electrochemical technique used for characterizing the electrochemical properties of materials, particularly electrocatalysts. During CV, the potential of a working electrode is cycled between a set lower and upper limit, while the resulting current is measured. This method provides critical information on redox reactions, electron transfer kinetics, and the stability of materials. In electrocatalyst development, CV is commonly used for the pretreatment of electrodes to improve their catalytic performance by cleaning the surface, removing passivating oxide layers, or restructuring the catalyst at the atomic level. Through controlled potential scanning, electrocatalysts can be activated or stabilized, which enhances their overall efficiency and longevity in electrochemical reactions.

3.1.2.2 Comparison of current density before and after CV pretreatment on electrocatalysts

The comparison of current density before and after CV pretreatment provides key insights into the impact of cyclic voltammetry on electrocatalyst performance. Current density is a direct indicator of the catalytic activity, as it reflects the number of electrons involved in the reaction per unit area of the electrode surface. Before pretreatment, electrocatalysts often show lower current densities due to surface impurities, passivation layers, or insufficient surface activation. After CV pretreatment, an increase in current density is typically observed, indicating improved electrocatalytic activity. This enhancement is attributed to the removal of surface contaminants, exposure of active sites, or restructuring of the catalyst surface, which increases the number of available sites for electron transfer and reaction. The comparison of pre- and post-treatment current densities helps to quantify the effectiveness of CV pretreatment in enhancing the electrocatalytic performance.

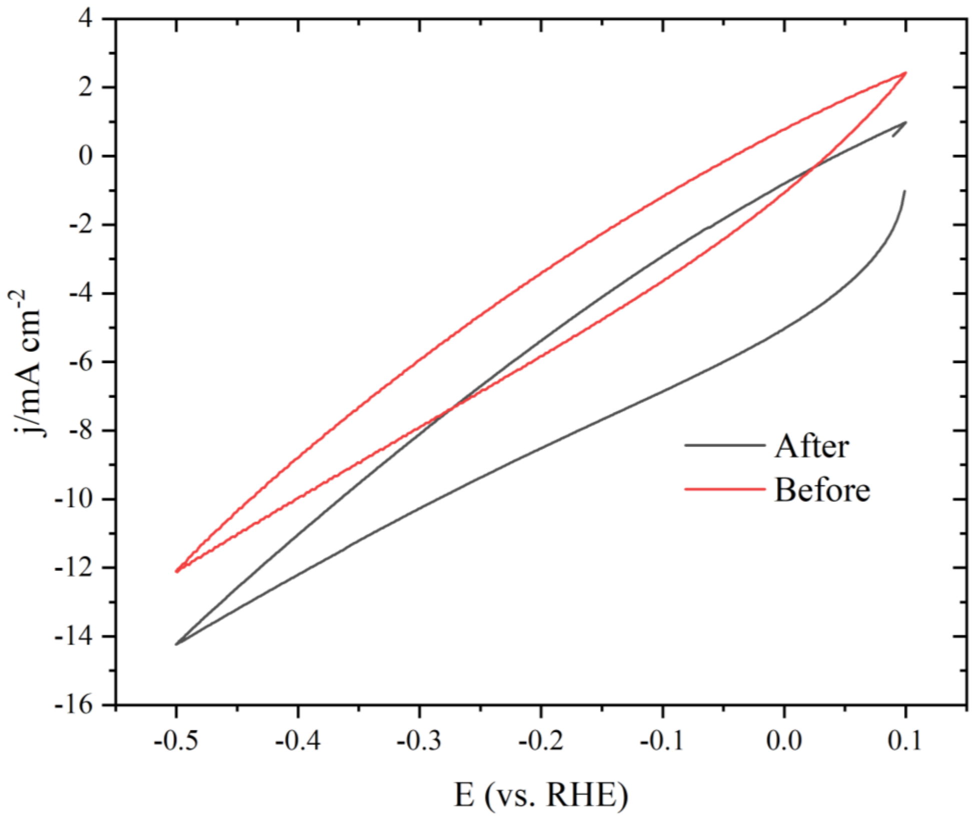

Figure 3.1. The current density change after CV pretreatment as catalyst activation (Pd/C as example here).

3.2 Facility and Parameters Applied in the Experiments

3.2.1 Potentiostat

A potentiostat, illustrated in Figure 2.1, is a specialized electronic device employed in electrochemistry to manage the voltage difference between a working electrode (WE) and a reference electrode (RE), while also recording the current that flows through the counter electrode (CE). These instruments are integral to various electrochemical investigations such as corrosion analysis, electroplating, battery development, and electroanalytical chemistry. Potentiostats are known for their high precision, enabling scientists to meticulously control and accurately measure electrochemical reactions.

Figure 3.2 Image of Metrohm potentiostat PGSTAT128N.

3.2.2 Linear Sweep Voltammetry (LSV)

In electrocatalysis, Linear Sweep Voltammetry (LSV) provides critical insights into the electrocatalytic activity and stability of materials. By analyzing the current-voltage curve obtained from an LSV experiment using a potentiostat, researchers can determine key parameters such as onset potential, peak potential, and current density, which are essential for evaluating the performance of electrocatalysts. LSV data typically reflect the response of the current to a steadily applied potential at a slow scan rate of 1-5 mV/s. Here, the applied potential can be calculated using the equation:

$$E_{RHE} = E_{REF} + E_{REF^{o}} + 0.059pH$$

3.2.3 Faradaic Efficiency (FE)

Faradaic Efficiency (FE) is a measure of the efficiency of an electrochemical process in converting electrical energy into chemical energy, or vice versa. It is expressed as a percentage and is typically determined by measuring the amount of product generated or reactant consumed during an electrochemical reaction and comparing it to the amount of charge passed through the system. In an electrolysis reaction, FE is calculated as the ratio of the amount of product generated by the desired reaction to the total amount of charge passed through the system. An FE of 100% indicates that all electrical energy was used to drive the desired reaction, while a lower efficiency indicates that some energy was lost due to Ohmic resistance, mass transport, kinetic losses, or other undesired products[2].

The standard equation for calculating the FE of the products is defined as follows:

$$FE_i = \frac{N_i Z_j F}{Q} \times 100\%$$

where N_i is the number of moles of product i, Z_i is the number of electrons transferred per molecule of product, F is the Faraday constant (96485.3 C/mol), and Q is the total charge passed through the system.

3.2.4 Gas Chromatography (GC)

Gas chromatography (GC) is a separation technique used to analyze and separate components of a gaseous mixture based on their ability to pass through columns packed with different sizes. It is widely used in analytical chemistry for identifying and quantifying components in a sample. In this dissertation, the Shimadzu GC-2014 (Figure 2.3) equipped with a thermal conductivity detector (TCD) has been used for the quantification of H2.

Figure 3.3 Image of Shimazu GC-2014

3.2.5 High-performance Liquid Chromatography (HPLC)

High-performance liquid chromatography (HPLC) is a chromatographic technique used to separate and analyze compounds in an aqueous mixture. It involves passing a mixture through a column packed with a stationary phase and a mobile phase, where the compounds are separated based on their interactions with the stationary phase. In this project, liquid-phase products were analyzed using an HPLC (Shimadzu, LC20-AD) (Figure 2.3) equipped with a C18 column (Luna Omega, Phenomenex) and a photodiode array (PDA) UV-Vis detector (Shimadzu, SPD-M20A) set to 275 nm for detecting for all products.

Figure 3.4 Image of Shimazu GC-2014.

3.2.6 Characterization of the Catalysts

By using different analytical instruments to observe the physical properties, active sites, and redox behavior of catalysts, we can understand the characteristics of the catalysts and further infer the relationsh ip between the catalysts and catalytic reactions. The characterization techniques used in this dissertation include analyzing the crystal structure of the catalysts with **X-ray diffraction (XRD)**; observing the crystal morphology of the catalysts with **transmission electron microscopy (TEM)**; measuring the metal content of the catalysts with **inductively coupled plasma atomic emission spectroscopy (ICP-AES)**; and determining the **electrochemical active surface area (ECSA)** of the metal on the electrodes.

3.2.6.1 X-ray Diffraction (XRD)

X-ray diffraction (XRD) involves directing a beam of X-rays at a sample, where they interact with the atoms and produce a diffraction pattern unique to the material's crystal structure. In this study, XRD measurements were conducted using an Empyrean Multipurpose X-ray diffractometer (Figure 2.4) with Cu Kα radiation (λ = 0.15406 nm), operating at 40 kV and 30 mA. The scans were performed at a rate of 0.05° per second, ranging from 20° to 80°.

Figure 3.5 Image of Empyrean Multipurpose X-ray diffractometer.

3.2.6.2 Transmission Electron Microscopy (TEM)

Transmission electron microscopy (TEM) is an advanced imaging method for examining the internal structure and morphology of materials at the nanoscale. In TEM, a high-energy electron beam is directed through a thin sample layer on a grid, and the image is formed by detecting the electrons that pass through the sample. For this dissertation, TEM images were captured using a FEI Tecnai Spirit operating at 120 kV (Figure 2.5).

Figure 3.6 Image of FEI Tecnai Spirit.

3.2.6.3 Inductively Coupled Plasma-Optical Emission Spectrometry (ICP-OES)

ICP-OES is an analytical method used to determine a sample's elemental composition. This technique uses an inductively coupled plasma to ionize the atoms in the sample, and then measures the light emitted as these ions return to their ground state. In this dissertation, ICP-OES analysis was performed using a PerkinElmer Avio-200 (Figure 2.6) to determine the metal loading amounts in the samples.

Figure 3.7 Image of PerkinElmer Avio-200.

3.3 General reaction cell for electrocatalytic hydrogenation reactions

3.3.1 Single Cell

A single cell is a basic electrochemical reactor where electrocatalytic hydrogenation reactions occur. In this setup, the cell consists of an anode, where oxidation reactions take place, and a cathode, where hydrogenation occurs. The reactant species are introduced to the working electrode (typically the cathode) where hydrogen ions (protons) or molecular hydrogen are electrochemically reduced, leading to the hydrogenation of the substrate. The electrolyte facilitates ion transport between the two electrodes, and an external power source applies the necessary voltage to drive the reaction. This type of setup is simple and is often used for screening electrocatalysts or studying reaction mechanisms in hydrogenation reactions.

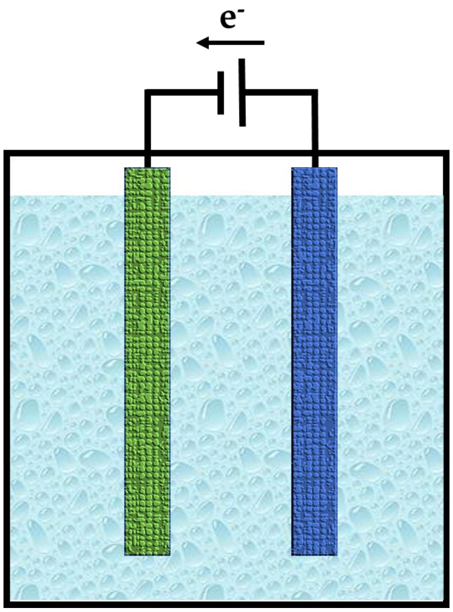

Figure 3.8 Image of typical single cell.

3.3.2 H-Cell

The H-cell setup is a two-compartment electrochemical cell, typically used for electrocatalytic hydrogenation reactions to physically separate the anode and cathode compartments. A porous frit or ion-permeable membrane separates the two compartments, allowing ionic conductivity while preventing the mixing of reactants and products between the compartments. In this configuration, the reactant to be hydrogenated is typically introduced to the cathode compartment, where the hydrogenation takes place, while the anode performs the oxidation of a suitable counter species. The H-cell is often used for reactions requiring separation of products from the oxidation and reduction processes or when the reaction intermediates need to be isolated or studied.

Our standard H-cell (as shown in Figure 3.9) is divided by a membrane, which is only for proton exchange crossover. This setup has been used for determining the Faradaic Efficiency (FE) of products generated from the electrochemical reduction of nitroaromatic in this research. Liquid products in the compartment with the working electrode (WE) can be analyzed using high-performance liquid chromatography (HPLC) or nuclear magnetic resonance (NMR), while gaseous products can be analyzed using gas chromatography (GC). A cold trap (approximately ~ -20°C) is used to collect volatile products for analysis and to prevent these volatiles and solvents from entering the columns.

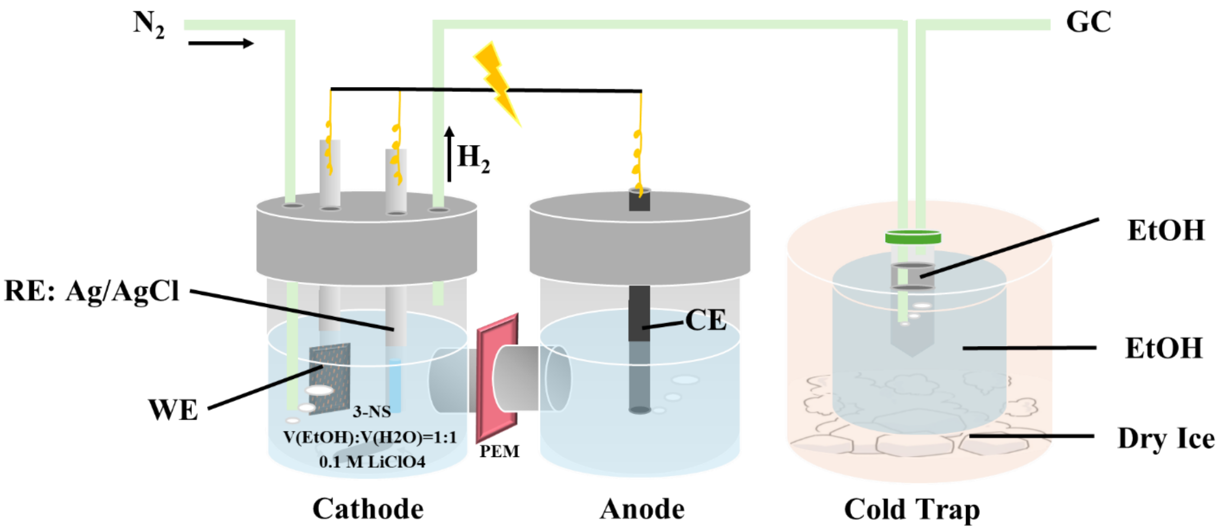

Figure 3.9 Schematic figure of our H-cell set-up

3.3.3 Membrane Electrode Assembly

The Membrane Electrode Assembly (MEA) is a more advanced setup, often used in proton exchange membrane (PEM) electrolyzers or fuel cells for electrocatalytic hydrogenation. In an MEA, the catalyst layers (anode and cathode) are directly coated or pressed onto a proton-conducting membrane, typically Nafion or a similar material. This membrane allows for proton (H^+) transport from the anode to the cathode, where the hydrogenation reaction takes place. The MEA design minimizes ion diffusion resistance and maximizes efficiency by ensuring close contact between the catalyst, membrane, and reactants. This setup is highly efficient for hydrogenation reactions, especially in proton-based electrocatalytic systems, and is commonly used in industrial applications for hydrogenation and fuel cell technologies. The MEA configuration is advantageous for scaling up reactions due to its compact, efficient, and easily controllable nature.

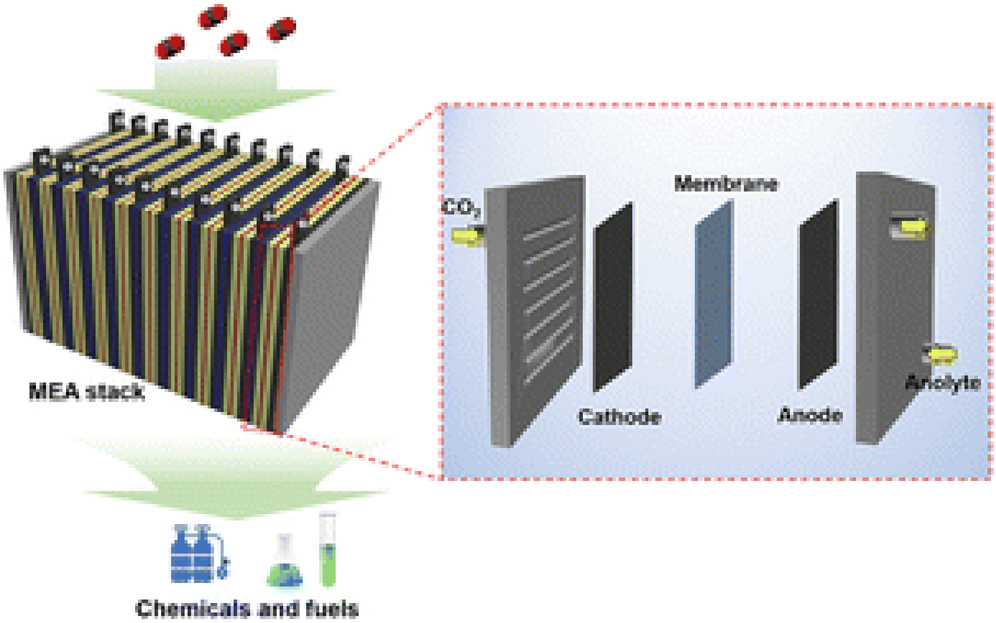

Figure 3.10 Image of typical MEA[3].

3.4 Raw data

3.4.1 Calibration curves

For the liquid product, we tested the product concentration at the cathode and anode ends by HPLC. The electroreduction reaction mainly occurs at the cathode end, so most of the product and the remaining substrate are mainly at the cathode end. The proton transfer membrane will cause some substrates to crossover to the anode end, and this part of the substrate does not react, so we also tested the anode end.

The HPLC callibration curve is composed of different concentrations of 3-NS, 3VA, 3EA, and 3-EN. The concentration gradients are 3-NS: 0.377mM, 0.754 mM, 1.509 mM, 3.018 mM, 3.772 mM; 3-VA: 0.814 mM, 1.628 mM, 3.256 mM, 4.07 mM; 3-EA: 0.408 mM, 0.816 mM, 1.633 mM, 3.266 mM, 4.082 mM; 3-EN: 0.314 mM, 0.628 mM, 1.257 mM, 2.514 mM, 3.142 mM. The specific chart is as follows.

The GC callibration curve is composed of N2 and H2 in different mixing ratios. The specific calculation can be seen in 2.2.6. The specific chart is as follows.

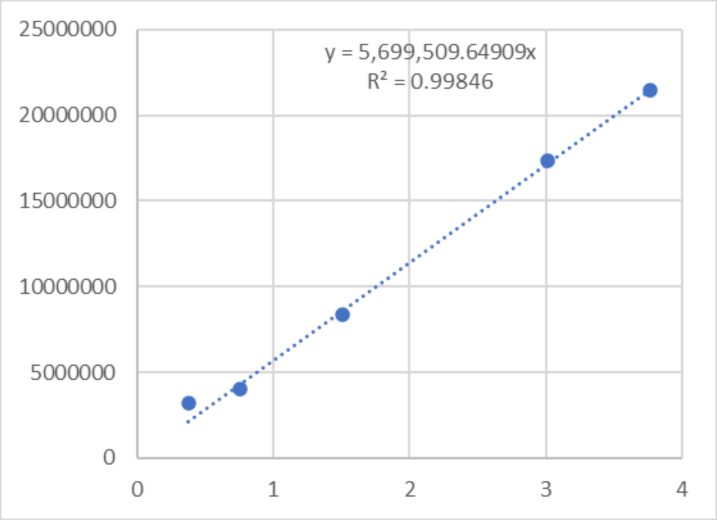

Figure 3.11 3-NS HPLC calibration curve.

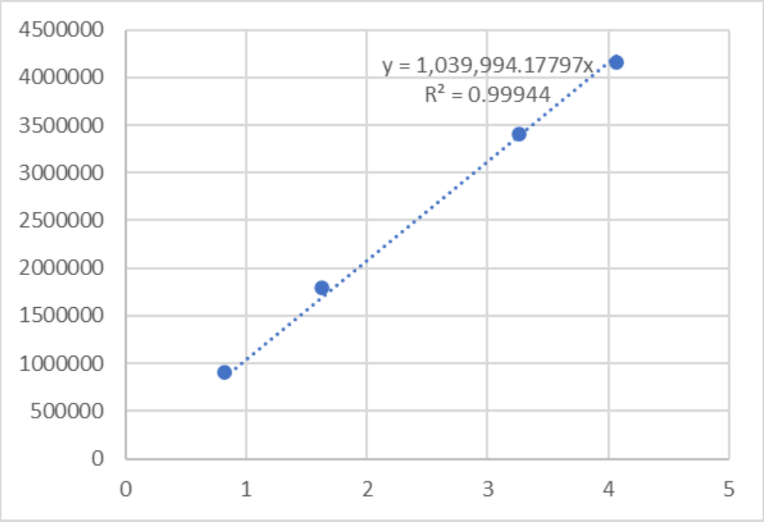

Figure 3.12 3-VA HPLC calibration curve.

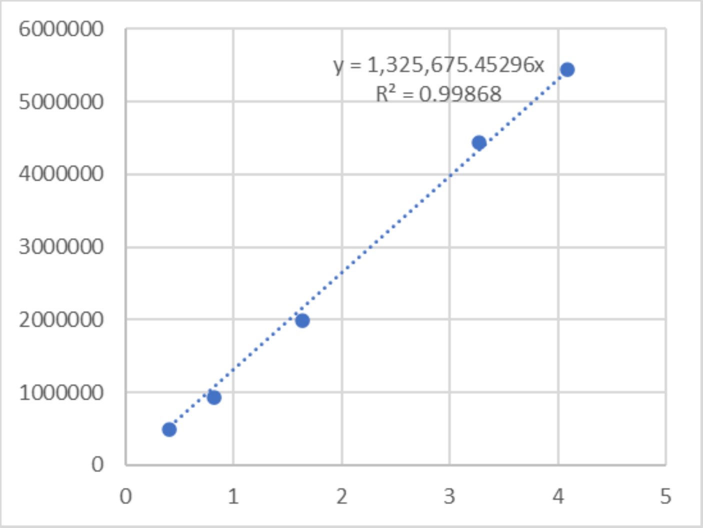

Figure 3.13 3-EA HPLC calibration curve.

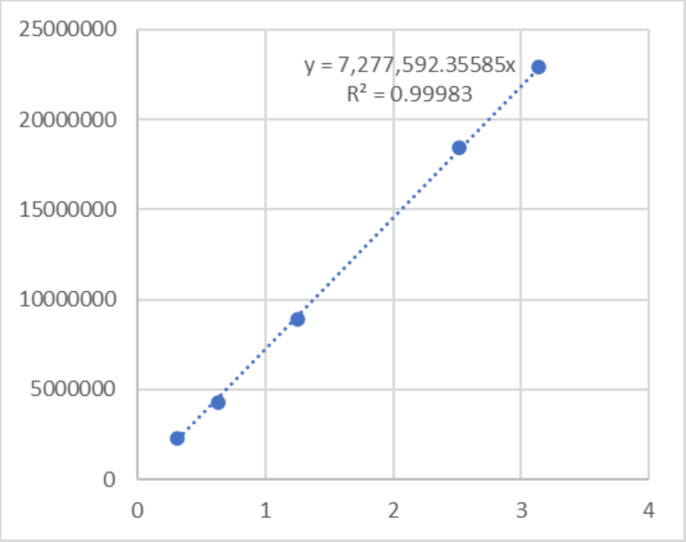

Figure 3.14 3-EN HPLC calibration curve.

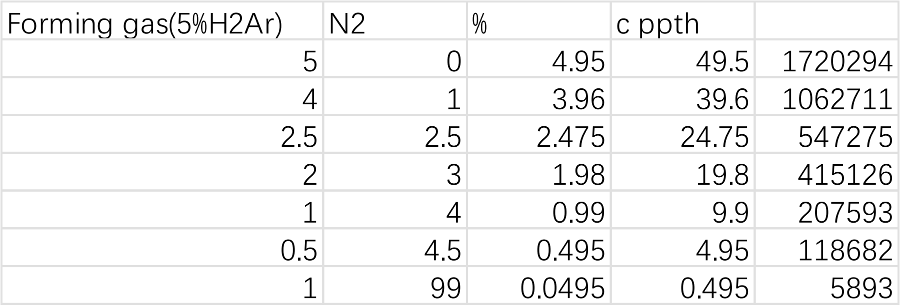

Forming gas(5%H2Ar)	N2	%	c ppth	
5	0	4.95	49.5	1720294
4	1	3.96	39.6	1062711
2.5	2.5	2.475	24.75	547275
2	3	1.98	19.8	415126
1	4	0.99	9.9	207593
0.5	4.5	0.495	4.95	118682
1	99	0.0495	0.495	5893

Table 3.1. Different ratios of H_2/N_2.

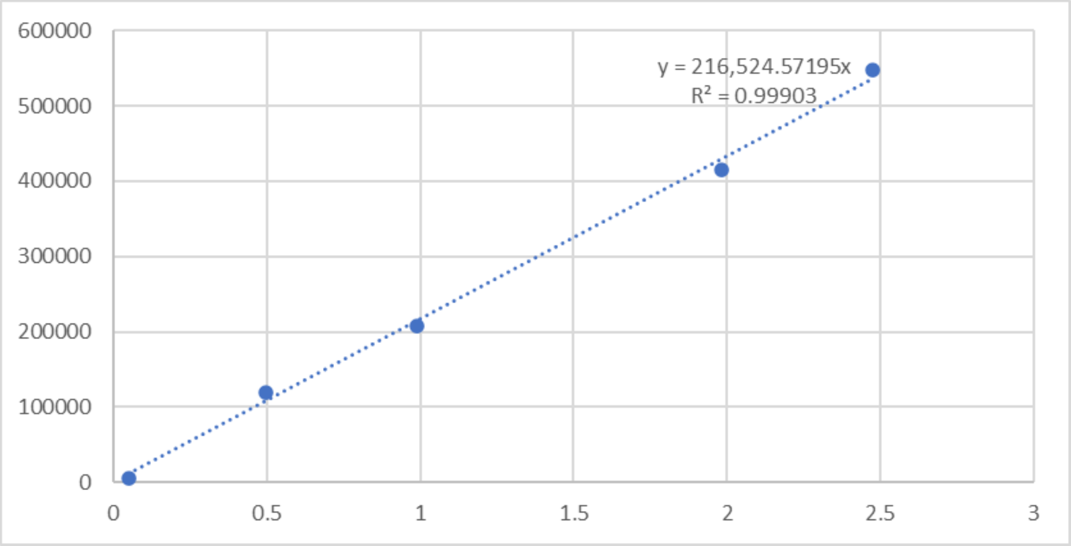

Figure 3.15 GC calibration curve.

3.4.2 HPLC raw data

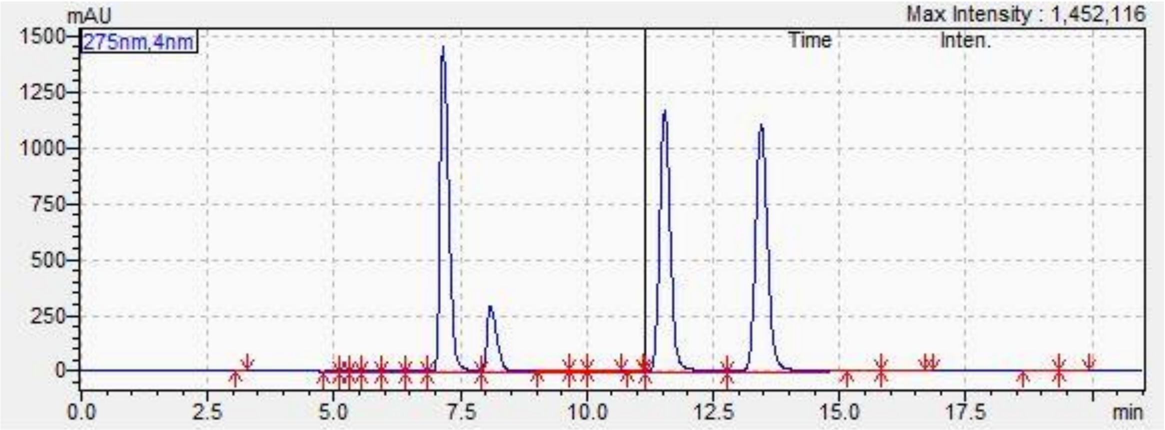

Figure 3.16 HPLC data of 100% 3-NS, 3-VA, 3-EA, and 3-EN.

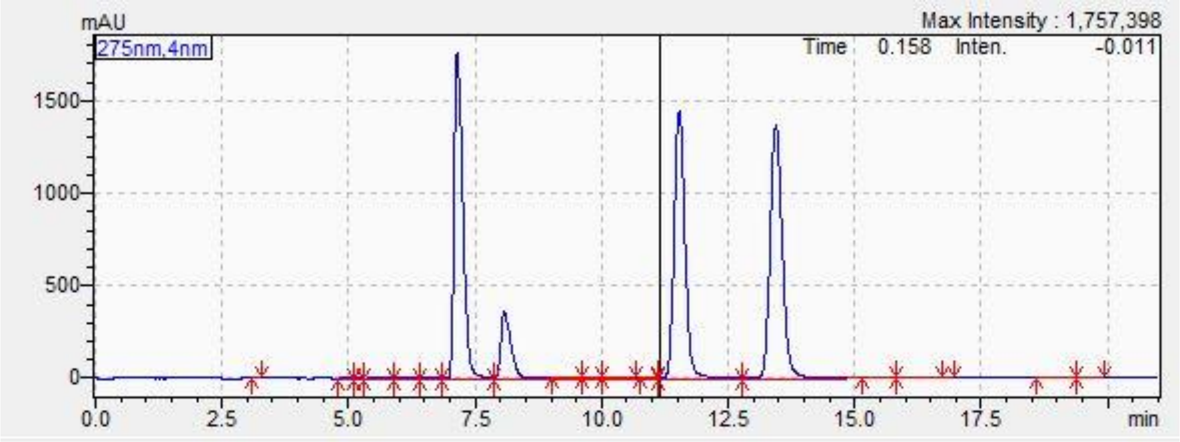

Figure 3.17 HPLC data of 80% 3-NS, 3-VA, 3-EA, and 3-EN.

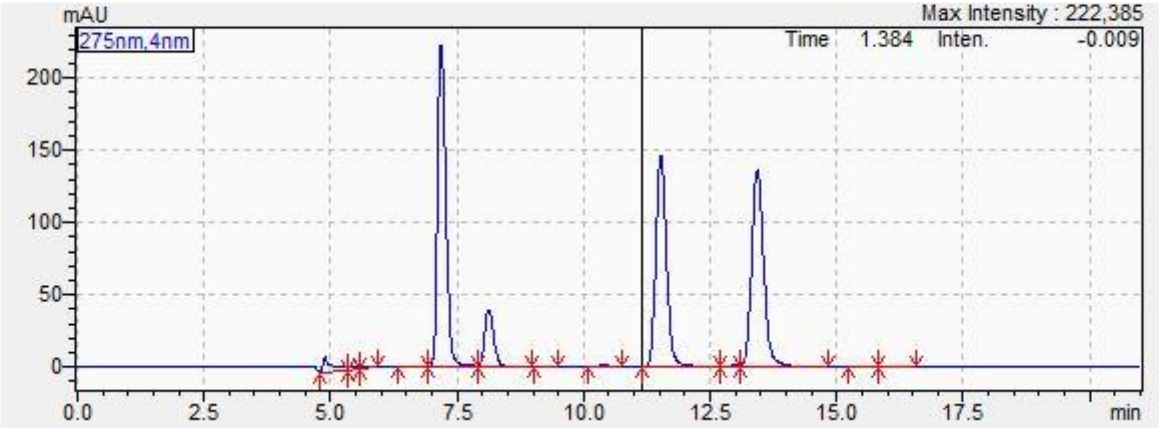

Figure 3.18 HPLC data of 40% 3-NS, 3-VA, 3-EA, and 3-EN.

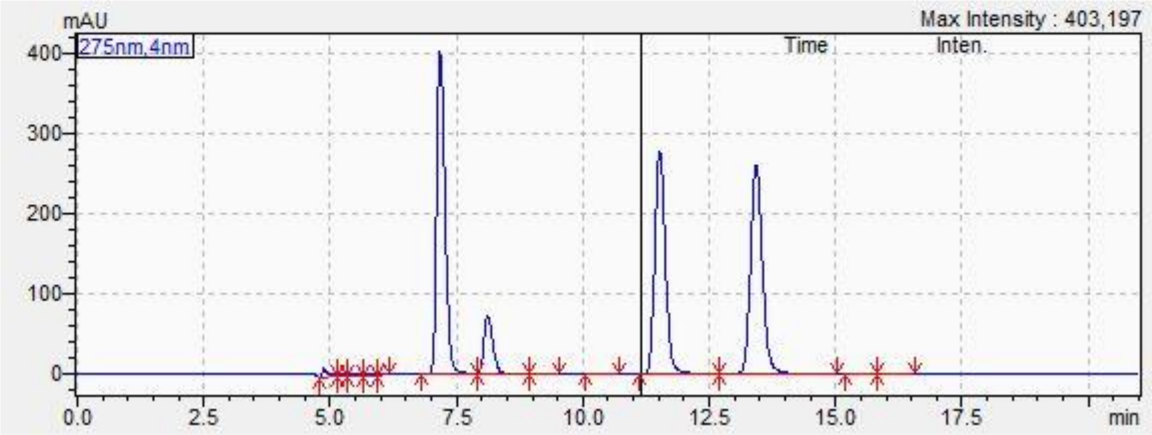

Figure 3.19 HPLC data of 20% 3-NS, 3-VA, 3-EA, and 3-EN.

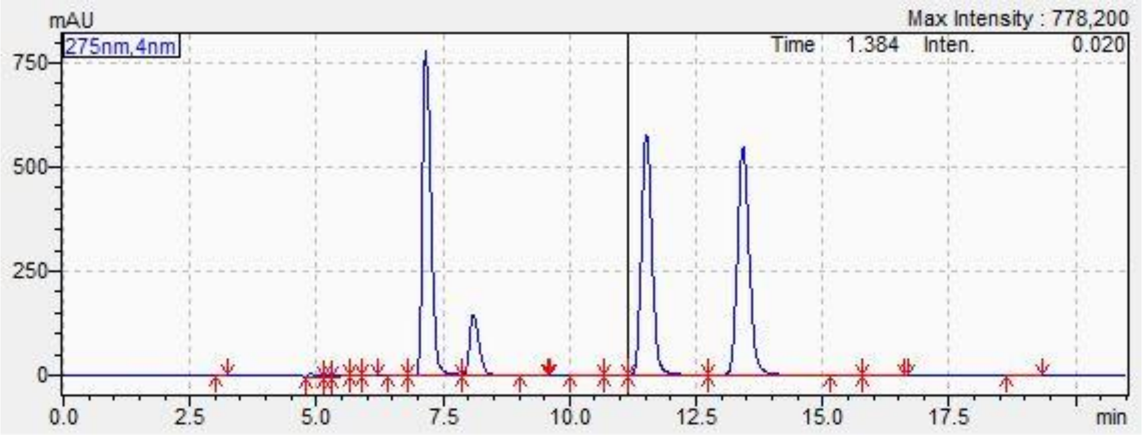

Figure 3.20 HPLC data of 10% 3-NS, 3-VA, 3-EA, and 3-EN.

Commercial Pd

pH=7; E (vs.RHE) = -0.45 V

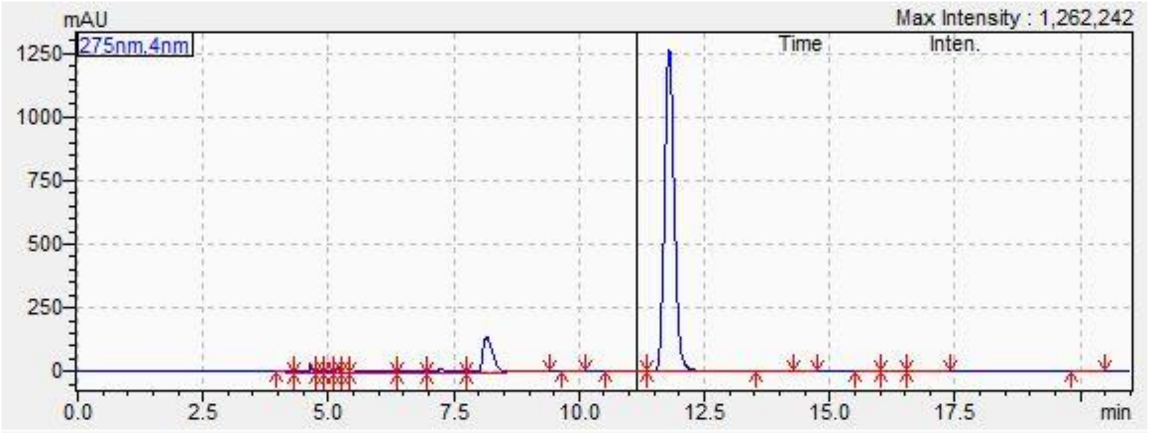

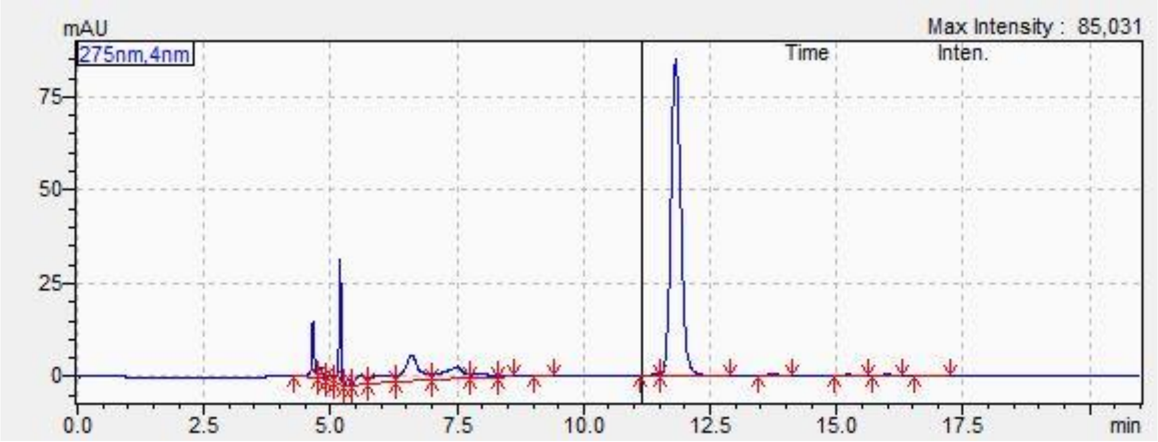

	3-NS	3-VA	3-EA	3-EN
Initial concentration (mM)	4.900	0	0	0
Crossover concentration (mM)	0.203			
Final concentration (mM)	3.010	0.187	1.420	0.008
Δ Concentration (mM)	1.687	0.187	1.420	0.008
Selectivity (%)		11.579	87.926	0.495
Carbon balance (%)	95.732			

pH=7; E (vs.RHE) = -0.30 V

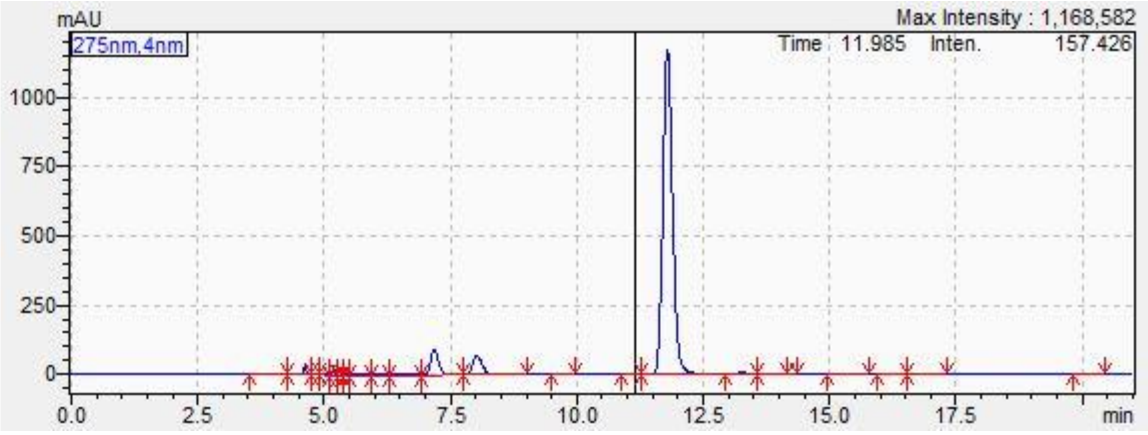

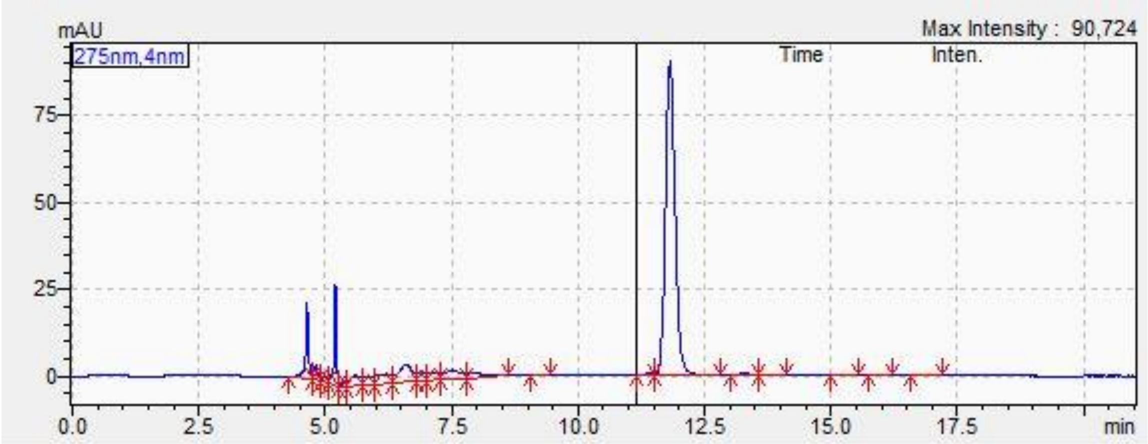

	3-NS	3-VA	3-EA	3-EN
Initial concentration (mM)	4.900	0	0	0
Crossover concentration (mM)	0.209			
Final concentration (mM)	2.728	1.230	0.715	0.014
Δ Concentration (mM)	1.963	1.230	0.715	0.014

Selectivity (%)		62.787	36.498	0.715
Carbon balance (%)	99.796			

pH=7; E (vs.RHE) = -0.15 V

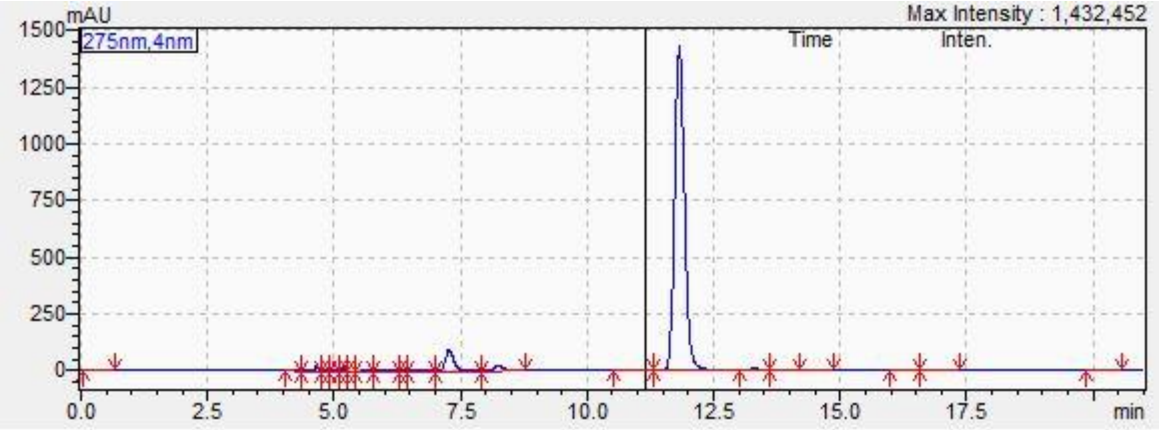

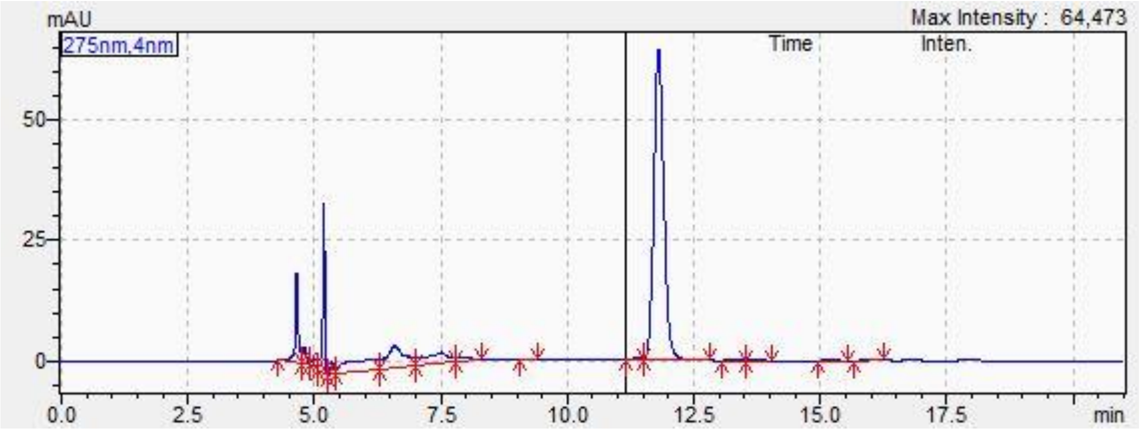

	3-NS	3-VA	3-EA	3-EN
Initial concentration (mM)	4.900	0	0	0
Crossover concentration (mM)	0.154			
Final concentration (mM)	3.428	1.023	0.215	0.014

Δ Concentration (mM)	1.318	1.023	0.215	0.014
Selectivity (%)		81.710	17.173	1.118
Carbon balance (%)	94.992			

pH=1; E (vs.RHE) = -0.45 V

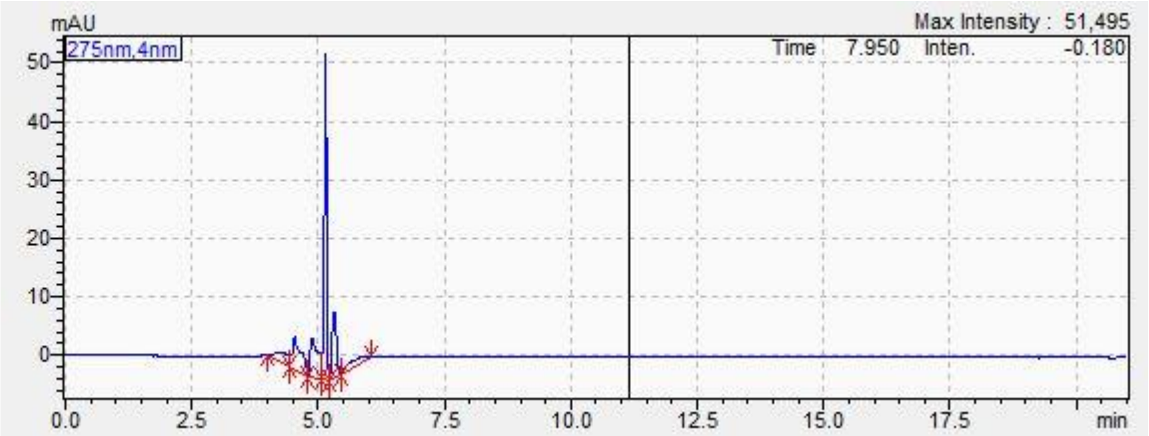

	3-NS	3-VA	3-EA	3-EN	Cold trap
Initial concentration (mM)	3.025	0	0	0	0
Crossover concentration (mM)	0				
Final concentration (mM)	0	0	0	0	2.998
Δ Concentration (mM)	0	0	0	0	2.998
Selectivity (%)		0	0	0	

Carbon balance (%)	0	

pH=1; E (vs.RHE) = -0.30 V

	3-NS	3-VA	3-EA	3-EN	Cold trap
Initial concentration (mM)	3.025	0	0	0	0
Crossover concentration (mM)	0.035				
Final concentration (mM)	0.083	0.038	0.660	0.028	2.154
Δ Concentration (mM)	0.753	0.038	0.660	0.028	2.154
Selectivity (%)		5.234	90.909	3.857	
Carbon balance (%)	96.415				

pH=1; E (vs.RHE) = -0.15 V

	3-NS	3-VA	3-EA	3-EN	Cold trap

Initial concentration (mM)	3.025	0	0	0	0
Crossover concentration (mM)	0.046				
Final concentration (mM)	0.113	0.380	0.940	0.004	1.428
Δ Concentration (mM)	1.438	0.380	0.940	0.004	1.428
Selectivity (%)		28.701	70.997	0.302	
Carbon balance (%)	92.072				

pH=14; E (vs.RHE) = -0.45 V

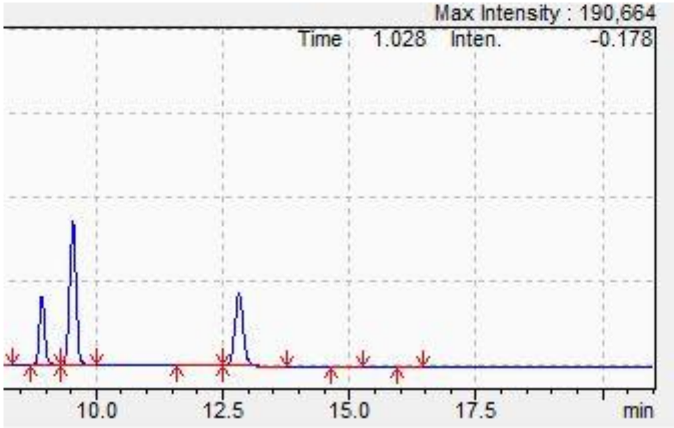

	3-NS	3-VA	3-EA	3-EN
Initial concentration (mM)	4.060	0	0	0
Crossover concentration (mM)	0.052			

Final concentration (mM)	0.770	0.380	2.832	0.041
Δ Concentration (mM)	3.238	0.380	2.832	0.041
Selectivity (%)		11.682	87.058	1.260
Carbon balance (%)	100.463			

pH=14; E (vs.RHE) = -0.30 V

	3-NS	3-VA	3-EA	3-EN
Initial concentration (mM)	4.060	0	0	0
Crossover concentration (mM)	0.212			
Final concentration (mM)	1.680	0.594	1.592	0
Δ Concentration (mM)	2.168	0.594	1.592	0
Selectivity (%)		27.173	72.827	0
Carbon balance (%)	100.830			

pH=14; E (vs.RHE) = -0.15 V

	3-NS	3-VA	3-EA	3-EN
Initial concentration (mM)	4.060	0	0	0
Crossover concentration (mM)	0.179			

Final concentration (mM)	1.482	1.642	0.725	0
Δ Concentration (mM)	2.399	1.642	0.725	0
Selectivity (%)		69.37	30.629	0
Carbon balance (%)	98.666			

Commercial Pt

pH=7; E (vs.RHE) = -0.45 V

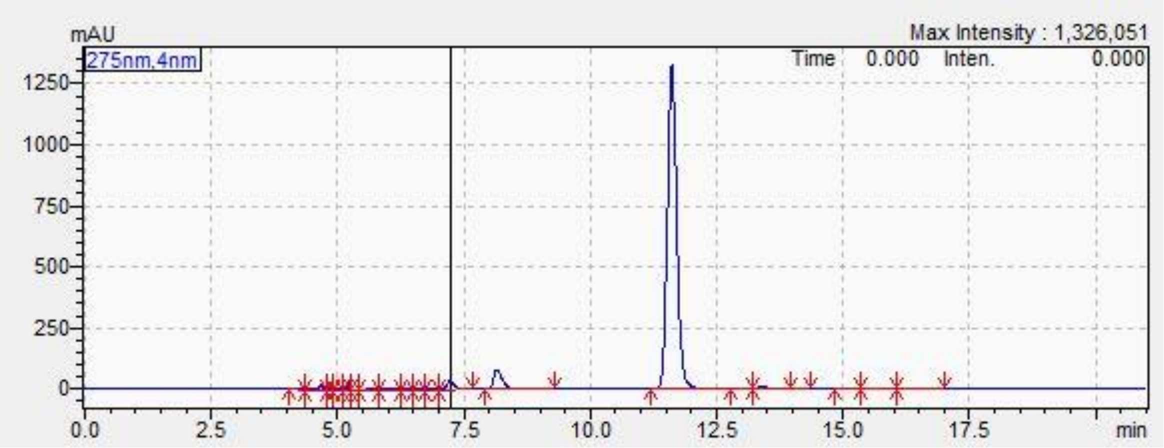

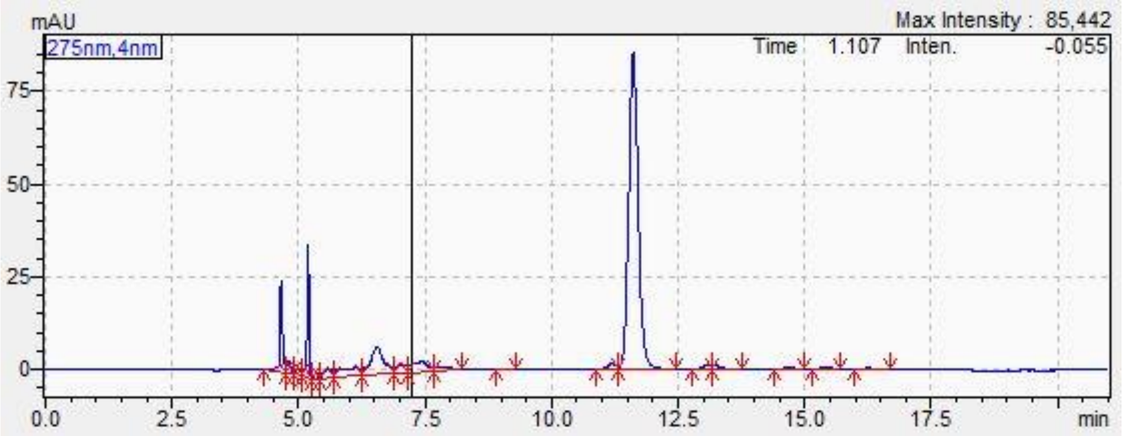

	3-NS	3-VA	3-EA	3-EN
Initial concentration (mM)	5.000	0	0	0
Crossover concentration (mM)	0.198			
Final concentration (mM)	3.031	0.624	1.134	0.025
Δ Concentration (mM)	1.771	0.624	1.134	0.025
Selectivity (%)		34.997	63.601	1.402
Carbon balance (%)	100.678			

pH=7; E (vs.RHE) = -0.30 V

	3-NS	3-VA	3-EA	3-EN
Initial concentration (mM)	5.000	0	0	0
32.071Crossover concentration (mM)	0.347			
Final concentration (mM)	2.910	1.097	0.525	0.015
Δ Concentration (mM)	1.743	1.097	0.525	0.015
Selectivity (%)		67.013	32.071	0.916
Carbon balance (%)	93.919			

pH=7; E (vs.RHE) = -0.15 V

	3-NS	3-VA	3-EA	3-EN
Initial concentration (mM)	5.000	0	0	0
Crossover concentration (mM)	0.095			
Final concentration (mM)	3.460	1.210	0.198	0.028
Δ Concentration (mM)	1.445	1.210	0.198	0.028
Selectivity (%)		84.262	13.788	1.950
Carbon balance (%)	99.377			

CuPd

pH=7; E (vs.RHE) = -0.45 V

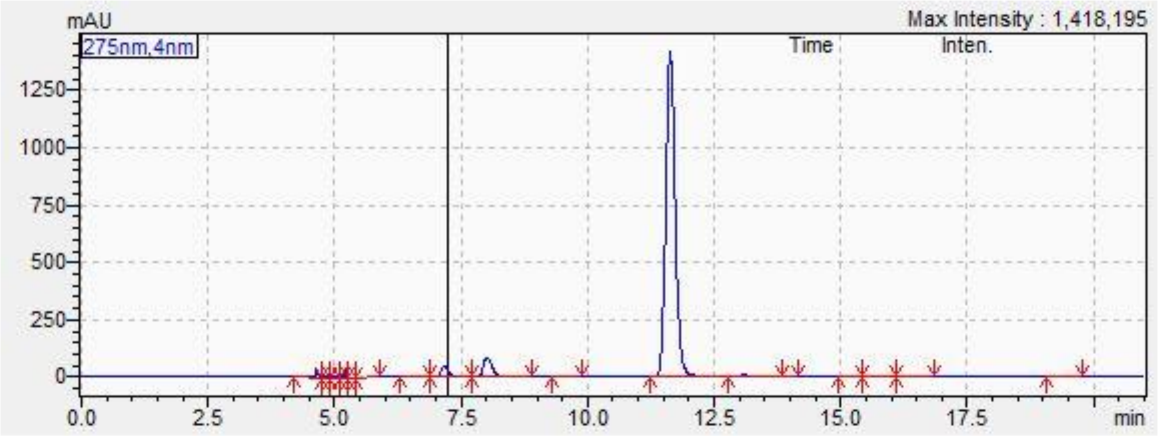

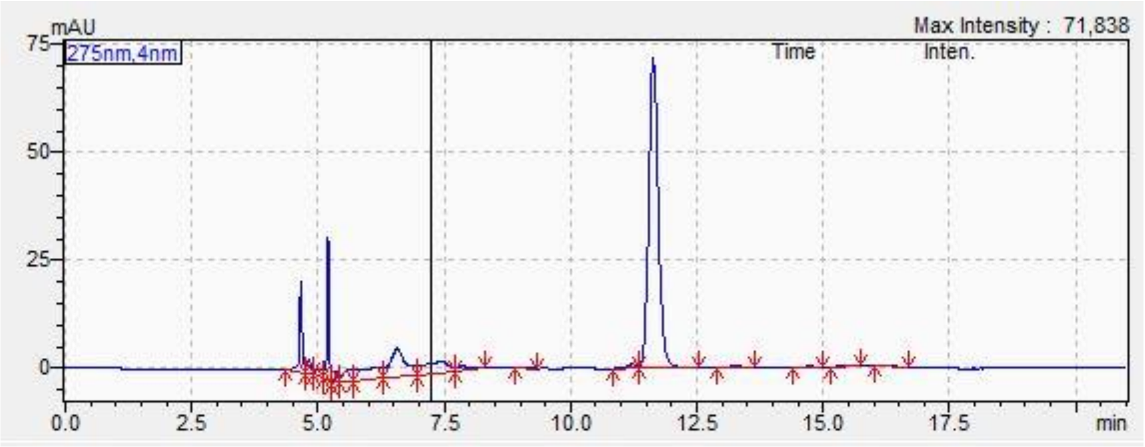

	3-NS	3-VA	3-EA	3-EN
Initial concentration (mM)	5.000	0	0	0
Crossover concentration (mM)	0.168			
Final concentration (mM)	3.230	0.770	0.822	0.015
Δ Concentration (mM)	1.602	0.770	0.822	0.015
Selectivity (%)		47.915	51.151	0.933
Carbon balance (%)	100.312			

CoPt

pH=7; E (vs.RHE) = -0.45 V

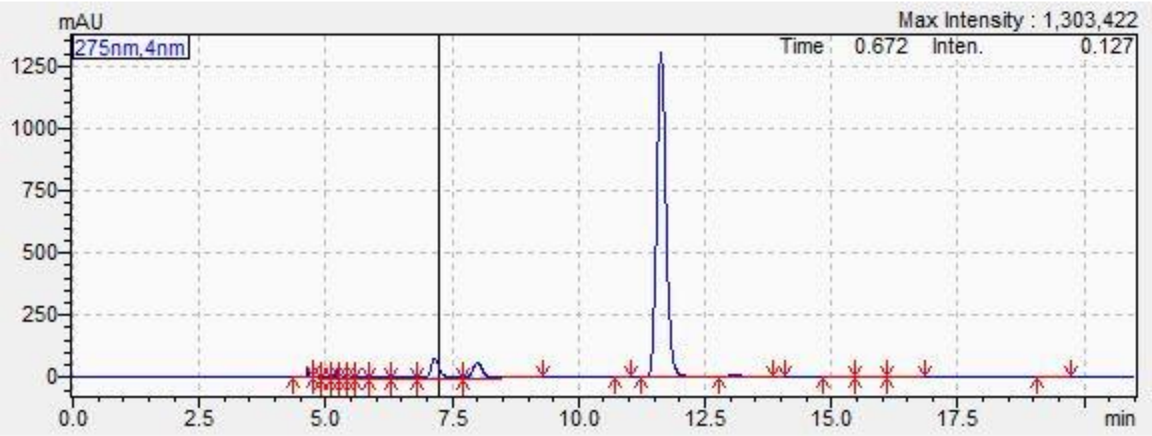

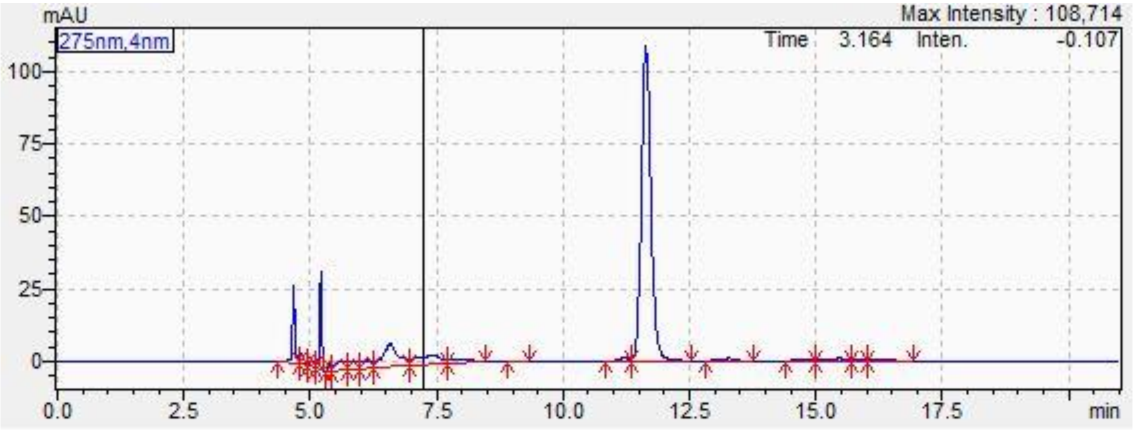

	3-NS	3-VA	3-EA	3-EN
Initial concentration (mM)	5.000	0	0	0
Crossover concentration (mM)	0.178			
Final concentration (mM)	2.592	1.195	0.772	0.017
Δ Concentration (mM)	2.230	1.195	0.772	0.017
Selectivity (%)		60.23	38.911	0.857
Carbon balance (%)	88.969			

Co_2P/Pt

pH=7; E (vs.RHE) = -0.45 V

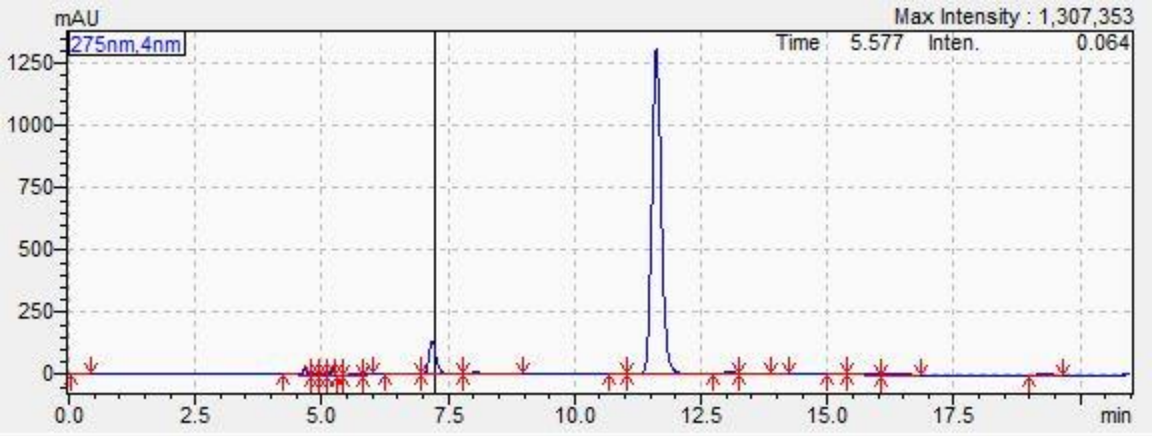

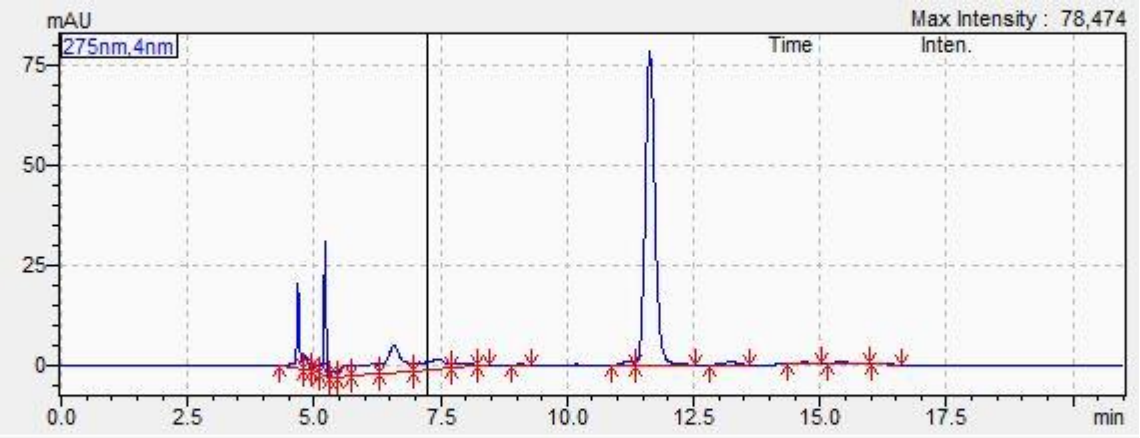

	3-NS	3-VA	3-EA	3-EN
Initial concentration (mM)	5.000	0	0	0
Crossover concentration (mM)	0.150			
Final concentration (mM)	3.105	1.449	0.255	0.010
Δ Concentration (mM)	1.745	1.449	0.255	0.010

Selectivity (%)		84.539	14.877	0.583
Carbon balance (%)	98.223			

Reference

1. Li, D.; Wang, C.; Tripkovic, D.; Sun, S.; Markovic, N. M.; Stamenkovic, V. R., Surfactant Removal for Colloidal Nanoparticles from Solution Synthesis: The Effect on Catalytic Performance. *ACS Catalysis* **2012,** *2* (7), 1358-1362.

2. Fornaciari, J. C.; Gerhardt, M. R.; Zhou, J.; Regmi, Y. N.; Danilovic, N.; Bell, A. T.; Weber, A. Z., The role of water in vapor-fed proton-exchange-membrane electrolysis. *Journal of The Electrochemical Society* **2020,** *167* (10), 104508.

3. Ye, Q.; Zhao, X.; Jin, R.; Dong, F.; Xie, H.; Deng, B., Advances and challenges in membrane electrode assembly electrolyzers for CO2 reduction. *Journal of Materials Chemistry A* **2023,** *11* (40), 21498-21515.